Single-step removal of arsenite ions from water through oxidation-coupled adsorption using Mn/Mg/Fe layered double hydroxide as catalyst and adsorbent

Thi Hai Nguyen, Hai Nguyen Tran, Tien Vinh Nguyen, Saravanamuthu Vigneswaran, Van Tuyen Trinh, Thanh Dong Nguyen, Thi Hoang Ha Nguyen, Trong Nhuan Mai, Huan-Ping Chao

PII: S0045-6535(21)03844-3

DOI: https://doi.org/10.1016/j.chemosphere.2021.133370

Reference: CHEM 133370

To appear in: *ECSN*

Received Date: 21 February 2021

Revised Date: 12 December 2021

Accepted Date: 17 December 2021

Please cite this article as: Nguyen, T.H., Tran, H.N., Nguyen, T.V., Vigneswaran, S., Trinh, V.T., Nguyen, T.D., Ha Nguyen, T.H., Mai, T.N., Chao, H.-P., Single-step removal of arsenite ions from water through oxidation-coupled adsorption using Mn/Mg/Fe layered double hydroxide as catalyst and adsorbent, *Chemosphere* (2022), doi: https://doi.org/10.1016/j.chemosphere.2021.133370.

Author contributions

Thi Hai Nguyen: Conceptualization, Data curation, Formal analysis, Investigation, Writing-Original draft preparation. **Hai Nguyen Tran:** Conceptualization, Data curation, Formal analysis, Validation, Writing – review & editing. **Tien Vinh Nguyen:** Conceptualization, Funding acquisition, Supervision, Writing - review & editing. **Saravanamuthu Vigneswaran:** Funding acquisition, Writing - review & editing, Validation. **Van Tuyen Trinh:** Writing - review & editing. **Thanh Dong Nguyen:** Formal analysis, Writing - review & editing. **Thi Hoang Ha Nguyen:** Formal analysis, Writing - review & editing. **Trong Nhuan Mai:** Writing - review & editing. **Huan-Ping Chao:** Formal analysis, Validation.

Graphical abstract

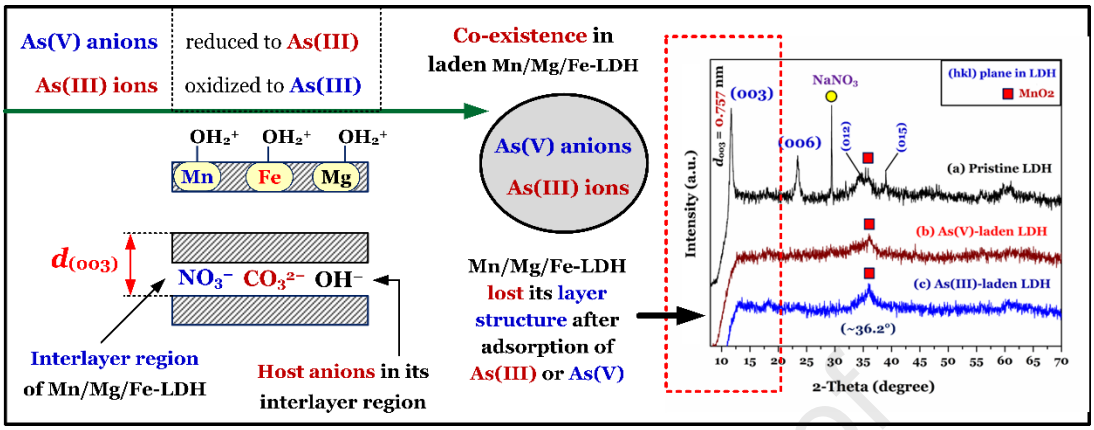

Single-step removal of arsenite ions from water through oxidation-coupled adsorption using Mn/Mg/Fe layered double hydroxide as catalyst and adsorbent

Thi Hai Nguyen[1], Hai Nguyen Tran[2,3*], Tien Vinh Nguyen[1]*, Saravanamuthu Vigneswaran[1], Van Tuyen Trinh[4], Thanh Dong Nguyen[4], Thi Hoang Ha Nguyen[5], Trong Nhuan Mai[5], Huan-Ping Chao[6]

[1]Faculty of Engineering and IT, University of Technology Sydney (UTS), Sydney, Australia

[2]Institute of Fundamental and Applied Sciences, Duy Tan University, Ho Chi Minh, 700000, Vietnam

[3]Faculty of Environmental and Chemical Engineering, Duy Tan University, Da Nang, 550000, Vietnam

[4]Institute of Environmental Technology, Vietnam Academy of Science and Technology, Hanoi, Vietnam

[5]VNU University of Science, Vietnam National University, Hanoi, Vietnam

[6]Department of Environmental Engineering and R&D Center for Membrane Technology, Chung Yuan Christian University, Taoyuan, 32023, Taiwan

---

***Corresponding authors:**

Email: trannguyenhai@duytan.edu.vn; trannguyenhai2512@gmail.com (H.N. Tran) and Tien.Nguyen@uts.edu.au (T.V. Nguyen)

Abstract

This study developed a layered double hydroxides (Mn/Mg/Fe-LDH) material through a simple co-precipitation method. The Mn/Mg/Fe-LDH oxidized arsenite [As(III)] ions into arsenate [As(V)] anions. The As(III) and oxidized As(V) were then adsorbed on Mn/Mg/Fe-LDH. The adsorption process of arseniate [As(V)] oxyanions by Mn/Mg/Fe-LDH was simultaneously conducted for comparison. Characterization results indicated that (i) the best Mg/Mn/Fe molar ratio was 1/1/1, (ii) the Mn/Mg/Fe-LDH structure was similar to that of hydrotalcite, (iii) the Mn/Mg/Fe-LDH possessed a positively charged surface (pH_{IEP} of 10.15) and low Brunauer–Emmett–Teller surface area (S_{BET} = 75.2 m^2/g), and (iv) Fe^{2+}/Fe^{3+} and $Mn^{2+}/Mn^{3+}/Mn^{4+}$ coexisted in Mn/Mg/Fe-LDH. The As(III) adsorption process by Mn/Mg/Fe-LDH was similar to that of As(V) under different experimental conditions (initial solutions pH, coexisting foreign anions, contact times, initial As concentrations, temperatures, and desorbing agents). The Langmuir maximum adsorption capacity of Mn/Mg/Fe-LDH to As(III) (56.1 mg/g) was higher than that of As(V) (32.2 mg/g) at pH 7.0 and 25 °C. X-ray photoelectron spectroscopy was applied to identify the oxidation states of As in laden Mn/Mg/Fe-LDH. The key removal mechanism of As(III) by Mn/Mg/Fe-LDH was oxidation-coupled adsorption, and that of As(V) was reduction-coupled adsorption. The As(V) mechanism adsorption mainly involved: (1) the inner-sphere and outer-sphere complexation with OH groups of Mn/Mg/Fe-LDH; and (2) anion exchange with host anions (NO_3^-) in its interlayer. The primary mechanism adsorption of As(III) was the inner-sphere complexation. The redox reactions made Mn/Mg/Fe-LDH loss its original layer structure after adsorbing As(V) or As(III). The adsorption process was highly irreversible. Mn/Mg/Fe-LDH can decontaminate As from real groundwater samples from 45–92 ppb to 0.35–7.9 ppb (using 1.0 g/L). Therefore, Mn/Mg/Fe-LDH has great potential as a material for removing As.

Keywords: Arsenic removal; Layer Double Hydroxides; Oxidation-coupled adsorption; Reduction-coupled adsorption; Redox reaction; Water treatment.

1. Introduction

Arsenic (As), a naturally occurring ubiquitous element in groundwater, adversely affects the quality of drinking water throughout the world, and particularly in Bangladesh, India, China, and Vietnam (Smedley and Kinniburgh, 2002; Kim et al., 2011). Natural weathering processes and anthropogenic activities are the main reasons for the presence of As in groundwater. As is widely found in water environments where it exists as a naturally reductive or oxidative mechanism (Smedley and Kinniburgh, 2002; Lu et al., 2018). Arsenate [As(V)] and arsenite [As(III)] ions are two common forms of As species detected in natural water bodies. In essence, As(III) has a higher toxicity and mobility than As(V) in water environments (Neppolian et al., 2008; Bagherifam et al., 2014). Exposure over a long period of time to contaminated As drinking water can seriously harm people's health including dermal, nervous, and other body systems (Berg et al., 2001). Many water treatment technologies have been devised to remove As from aquatic environments, such as adsorption (Nguyen et al., 2020), biological treatment (Lièvremont et al., 2009), and membrane process (Regis et al., 2022). Of the current existing technologies at a decentralized scale, adsorption is considered the most appropriate method due to its impressive removal efficiency, simple design, cost-effectiveness, and minimal secondary waste generation. Although activated carbon (AC) and biochar have been commonly used in water treatment, it has a low adsorption capacity to As(III) and As(V) in water. For this reason, it is necessary to make additional modifications or improve treatment, such as alumina composite-modified AC (Karmacharya et al., 2016), aluminum-enriched biochar (Ding et al., 2018), biochar modified with Fe/Mn (Lin et al., 2017), and the composite of Fe/Mn-LDH and carbon material (Fe/Mn-C-LDH) (Wang et al., 2021). As a result, the preparation costs of this material rise, and the two stage-preparation is very time-consuming.

Among existing adsorbents, layered double hydroxides (LDHs) have garnered much attention for the removal of both toxic cations and anions in aquatic environments due to their unique properties and simple synthesis processes (Asiabi et al., 2017; Wang et al., 2018; Tran

et al., 2019). The LDHs belong to the synthetic clay group, one that possesses different ionic layer structures such as positively charged brucite like layers and non-framework charge compensating anions in their galleries. Specifically, the form of LDH can be expressed by the general formula $[M^{2+}_{1-x}M^{3+}_{x}(OH)_2]^{x+}(A^{n-})_{x/n}\bullet mH_2O$. In this formula, M^{2+} and M^{3+} are divalent metal cations (i.e., Mg^{2+}, Cu^{2+}, Zn^{2+}, Ni^{2+}, and Fe^{2+}) and trivalent metal cations (Al^{3+} and Fe^{3+}) in the brucite like layers, respectively. A^{n-} indicates the interlayer charge (NO_3^-, CO_3^-, Cl^-, etc.), and x is the $M^{3+}/(M^{2+} + M^{3+})$ molar ratio (Huang et al., 2015; Pavlovic et al., 2016; Wang et al., 2018; Tran et al., 2019). Therefore, the positive charge of the material's brucite layers can efficiently react with toxic anions through electrostatic-attraction mechanism. Meanwhile, the host anions in the interlayer regions (i.e., CO_3^{2-} and NO_3^{2-} anions) demonstrate a very high exchange with toxic anions in solution (Asiabi et al., 2017; Hudcová et al., 2017; Mubarak et al., 2018; Wang et al., 2018; Varga et al., 2021).

Unlike As(V), As(III) exists as neutral molecular forms (without any charge; $H_3AsO_3^o$ ions) with solution pH from 0 to 8.0 (Figure S1) (Hudcová et al., 2017; Nguyen et al., 2020), so the adsorption of As(III) using layered double hydroxides through their positively charged surface or host anions in their interlayer region might not be feasible. Some authors transformed As(III) into As(V) by using some oxidizing agents, and removed As(V) from water (also known as a two-step removal process). For example, Neppolian et al. (2008) applied peroxydisulfate ions to effectively oxidize As(III) into less toxic As(V) anions. However, after the oxidation process a further removal process (i.e., adsorption or coagulation) is required. To solve this problem, some researchers developed a material that exhibited advantageous properties (acting as oxidant and adsorbent) to remove both As(III) and As(V) from water. A one-step removal process of both As(III) and As(V) using Fe(II)/Mn(II) oxides was reported by Bai et al. (2016). Herein, As(III) ions in solution were firstly oxidized into As(V) anions when it contacted the Fe(II)/Mn(II) oxides; subsequently, oxidized As(V) and As(III) in solution were adsorbed by

this oxide material. This removal process involved a combination of mechanisms, namely oxidation-coupled adsorption.

Most previous studies on As removal by LDH-based adsorbents focused on As(V) (Wang et al., 2009; Huang et al., 2015; Asiabi et al., 2017; Hudcová et al., 2017). This is because of the high anion-exchange capacity of such materials (Wang et al., 2018; Tran et al., 2019). Bagheriham et al. (2014) prepared Zn/Al-LDH and applied it to remove arsenite and arsenate from solution. Their findings showed that Zn/Al-LDH has a higher adsorption capacity of As(V) than toxic As(III). This is due to the nature of metal salts (Zn and Al) employed during the synthesis of LDH. In other words, the removal of toxic As(III) by the LDH-based materials is still a big challenge.

In this study, a clay-like sample (Mn/Mg/Fe-LDH) was simply prepared from three metals (Mn, Mg, and Fe) through a one-step coprecipitation process. The Mn and Fe metals were selected because their oxides have been acknowledged as effective oxidants to convert As(III) to As(V). The prepared Mn/Mg/Fe-LDH material was well characterized by various techniques and then applied to remove As(III) and As(V) from aqueous solution. The effect of important operating parameters (such as solution pH, contact time, temperature, etc.) which have strong impacts on the adsorption process were tested under batch experiments. The adsorption mechanisms were also discussed.

2. Material and methods

2.1. Reagents

All the chemicals and reagents used in this work were of an analytical grade and used without any further purification. $Mg(NO_3)_2 \cdot 6H_2O$ (256.4 g/mol), $Mn(NO_3)_2$, $Fe(NO_3)_3 \cdot 9H_2O$ (404 g/mol), sodium hydroxide NaOH, and sodium carbonate $NaCO_3$ were obtained from Sigma-Aldrich. Stock solutions of As(III) and As(V) were prepared by dissolving sodium

arsenite ($NaAsO_2$, from ACE Chemical Co.) and sodium arsenate heptahydrate ($Na_2HAsO_4•7H_2O$, from BDH Chemical Ltd.) in deionized water, respectively.

2.2. Synthesis of Mn/Mg/Fe layered double hydroxides

Manganese/magnesium/iron layered double hydroxides (Mn/Mg/Fe-LDH) were synthesized by co-precipitation method at different mass ratios of Mn/Mg/Fe, such as 2/1/1, 1/1/1, 2/1/2, and 1/1/2, respectively. The Mn/Mg/Fe sample prepared at the molar ratio of 1/1/1 was taken as a typical example. Namely, a 60 mL of the solution [containing 0.04 mol of $Mn(NO_3)_2$, 0.04 mol of $Mg(NO_3)_2•6H_2O$ and 0.04 mol of $Fe(NO_3)_3•9H_2O$] was added drop by drop into another 60 mL solution [containing 0.336 mol NaOH and 0.022 mol Na_2CO_3]. Continuous stirring was applied. The pH of the mixture was maintained at 12 ± 0.2 and aged at 45 °C for 3 h to maintain the precipitation. Le et al. (2009) reported that the Mg/Al-LDH precipitates were colloidal nanoparticles in solutions, with their average particle diameters ranging from 68.6 to 367 nm. The collected precipitate was centrifuged at 9000 rpm for 15 min. The concentrated precipitate was then washed several times with deionized water until the pH value of the filtrate reached a constant pH (approximately 7.0). The concentrated precipitate (Mn/Mg/Fe-LDH) was then dried at 80 °C for 48 h. After the drying process, the hard solids (~1.0–2.0 cm) were obtained because of the aggregation phenomenon of the Mn/Mg/Fe-LDH colloids. The hard solids were grinded and sieved into smaller particles (their sieve sizes ranging from 0.106 to 0.250 mm) and then stockpiled in tightly closed bags until further use. The other Mn/Mg/Fe samples at the molar ratios of 2/1/1, 2/1/2, and 1/1/2 were also synthesized in a similar way to that of Mn/Mg/Fe at 1/1/1.

A primary adsorption test (scanning experiment) was conducted to compare the adsorption capacity of Mn/Mg/Fe-LDH samples (prepared at four different molar ratios of Mn/Mg/Fe) with As(III) and As(V) solution. The adsorption conditions were fixed at 1.0 g/L of adsorbent dose, 24 h, 25 °C, pH = 7.0, and 3.5 mg/L of As(III) or As(V). The results (Figure S2) demonstrated that the Mn/Mg/Fe-LDH adsorbent prepared at the 1/1/1 ratio demonstrated

an efficiency in removing arsenic ions similar to that prepared at the 2/1/1 ratio and higher than that prepared at 1/1/2 and 2/1/1. Therefore, Mn/Mg/Fe-LDH adsorbent (prepared at a ratio of 1/1/1) was selected in the subsequent batch adsorption experiments and material characterization.

2.3. Characterization of Mn/Mg/Fe-LDH

The crystal phases of Mn/Mg/Fe-LDH were characterized using an X-ray Diffractometer (XRD; Empyrean-PANalytical). Its main functional groups were detected by Fourier transform infrared instrument (FTIR; Nicolet iS5). Morphological features and element composition of Mn/Mg/Fe-LDH were determined by scanning electron microscope coupled with energy-dispersive X-ray spectroscopy (SEM-EDS; Quanta-650). Its textural properties such as Brunauer-Emmett-Teller surface area (S_{BET}) and total pore volume (V_{Total}) were determined from the N_2 adsorption/desorption isotherm at 77 K (using Micromeritics sorptometer; AccuPyr II 1340. V1.02). The pH value at the isoelectric points (pH_{IEP}) of Mn/Mg/Fe-LDH was measured by a zeta potential analyser (Colloidal Dynamics; ZED-3600). The Mn/Mg/Fe-LDH solid has been degassed under vacuum conditions at 105 °C for 24 h before it was characterized.

2.4. Batch adsorption experiment

Arsenic adsorption onto Mn/Mg/Fe-LDH was studied under batch experiments at different operating parameters such as solution pH, contact time, initial As concentration, temperature, coexisting anion, and desorbing agent. All adsorption studies were done in triplicate. The values were presented as average ± standard deviation (as error bars).

The pH of the solution of As(III) or As(V) was firstly adjusted to 2.0 to 10.0 using 1.0 M NaOH and 1.0 M HNO_3. Approximately 0.1 g of Mn/Mg/Fe-LDH was added into a flask containing 100 mL of As(III) or As(V) solution. The solid/liquid (m/V) concentration of the adsorbent in this study amounted to 1.0 g/L. The flask was shaken using a mechanical shaker (Lab Tech LIS-2) at 150 rpm and 25 °C. After pre-determined shaking times, the solid and

liquid parts were separated and used for different tasks. The liquid was filtered through a 0.45 μm filter to analyse residual As in solution. The solid part was dried at 105 °C for 24 h and then stockpiled in tightly plastic bags for further characterization of laden Mn/Mg/Fe-LDH (i.e., FTIR, the textural, morphological properties, and desorption). The concentrations of As and other cations (Mn, Mg, or Fe leached from Mn/Mg/Fe-LDH during the adsorption process) in solution were determined by ICP-OES 7300 PerkinElmer. The amount of As adsorbed by Mn/Mg/Fe-LDH at any time (q_t; mg/g) and equilibrium (q_e; mg/g) was calculated by Equations 1 and 2, respectively.

$$q_t = \frac{(C_o - C_t)V}{m} \quad (1)$$

$$q_e = \frac{(C_o - C_e)V}{m} \quad (2)$$

where C_o, C_e, and C_t, are the concentrations (mg/L) of As in solution at beginning, equilibrium, and any time t (min), respectively; V is the volume of As solution applied; and m is the dried mass of Mn/Mg/Fe-LDH used.

A desorption study was carried out after the equilibrium adsorption process. Several desorbing agents were used for this purpose, such as Na_2CO_3 (0.2 M), NaCl (0.2 M), EDTA (0.2 M), NaOH (0.2 M), HCl (0.2 M), and deionized water (at pH = 12). After the adsorption process approximately 0.1 g of As-laden Mn/Mg/Fe-LDH was transferred into the flask containing 100 mL of each desorbing agent. The time set aside for the desorption study was 24 h at 25 °C.

More detailed information on the experiments involving the adsorption process is provided in Section S1. The experimental conditions of adsorption are summarized in the caption accompanying each figure.

3. Results and discussion

3.2. Characterization of Mn/Mg/Fe-LDH

3.2.1. Crystalline structure and surface morphology

The crystal structure of Mn/Mg/Fe-LDH is detected by X-ray powder diffraction. Figure 1 shows that Mn/Mg/Fe-LDH exhibited a typical structure of hydrotalcite-like material (Guo et al., 2017; Hudcová et al., 2017; Mubarak et al., 2018; Wang et al., 2021). This finding was confirmed from its morphology that was detected through SEM imaging (Figure S3). Two diffraction peaks (Figure 1) well-identified at 11.68° and 23.4° were regarded as the typical characteristics (the (003) and (006) planes, respectively) of LDH solid (Vucelic et al., 1997; Huang et al., 2015; Pavlovic et al., 2016; Tran et al., 2019; Zhang et al., 2022), suggesting that the LDH was successfully synthesized from three metal ions (Mn, Mg, and Fe). According to Bragg's law, the basal spacing (d_{003}) of Mn/Mg/Fe-LDH was 0.757 nm (Figure 1). The d_{003} value (0.757 nm) of Mn/Mg/Fe-LDH was similar to that of some other LDH materials reported in the literature, such as Mg/Fe-LDH (0.768 nm) (Vucelic et al., 1997), Mg/Al-LDH (0.781 nm) (Huang et al., 2015), and Mg/Fe-LDH (0.87 nm) (Mubarak et al., 2018).

Notably, a strong diffraction peak at 29.4° indicated the crystal nature of nitratite mineral ($NaNO_3$) (Córdova Reyes et al., 2014; Iruretagoyena Ferrer, 2016; Triviño et al., 2018) in the dried Mn/Mg/Fe-LDH. In addition, a peak at 36.2° might belong to the (110) plane of birnessite-type MnO_2 (Mohammadi et al., 2021). Those solids ($NaNO_3$ and MnO_2) that were naturally generated during the synthesis of Mn/Mg/Fe-LDH played an important role in adsorbing As(V) and As(III) in this study (Sections 3.10 and 3.11).

3.2.2. Textural property

The textural parameters of Mn/Mg/Fe-LDH were analysed by nitrogen adsorption/desorption isotherm (Figure 2). This physical sorption belongs to the Type IV isotherm and presents Type H3 hysteresis, suggesting that Mn/Mg/Fe-LDH was a mesoporous

material (average pore width ~14.2 nm) with slit-shaped pores (Tran et al., 2019; Varga et al., 2021; Wang et al., 2021). Mn/Mg/Fe-LDH exhibited a low BET surface area (S_{BET} = 75.2 m^2/g; **Figure 2**). This is a typical future of hydrotalcite like-materials such as Mg/Al-LDH (95.7 m^2/g) (Huang et al., 2015), Mn/Fe-LDH (82.6 m^2/g) (Wang et al., 2021), Ni/Al-LDH (61.05 m^2/g) (Asiabi et al., 2017), Mg/Zn/Fe-LDH (48.4 m^2/g) (Liu et al., 2019), Ca/Fe-LDH (43.3 m^2/g) (Lu et al., 2018), Mg/Fe-LDH (40.1 m^2/g) (Hudcová et al., 2017), and granular Mg/Fe-LDH (1.37 m^2/g) (Choong et al., 2021). This particular result suggests that the adsorption of arsenic ions onto Mn/Mg/Fe-LDH through pore-filing mechanism might be negligible.

3.2.3. Surface functionality

The main functional groups on the surface of Mn/Mg/Fe-LDH were identified by FITR. Figure 3 shows that a broad band at approximately 3430 cm^{-1} is attributed to the O–H stretching vibrations derived from the OH groups on the surface of Mn/Mg/Fe-LDH or from the OH^- anions on its interlayer region (Chubar et al., 2013; Lu et al., 2018). Meanwhile, the presence of Fe–O groups on the surface of Mn/Mg/Fe-LDH is typically identified at 594 cm^{-1} (Hudcová et al., 2017; Wang et al., 2021). Lastly, a band located at around 420 cm^{-1} is assigned to the M–O and M–OH vibrations (where M is Mg, Mn, or Fe), which is related to metal-oxygen bond and the metal hydrogen-oxygen stretching vibration (Huang et al., 2015; Asiabi et al., 2017).

Notably, an observed band at approximately 1384 cm^{-1} corresponds to the host anions in the interlayer region of Mn/Mg/Fe-LDH that is C=O (derived from CO_3^{2-} ions) (Huang et al., 2015; Hudcová et al., 2017; Wang et al., 2021) overlapped with N=O (NO_3^- ions) (Goh et al., 2008, 2009; Li et al., 2009; Chao et al., 2018). The identification of this band plays an important role in identifying the adsorption mechanisms in this study (Sections 3.10 and 3.11).

3.2.4. Chemical state of the main elements in Mn/Mg/Fe-LDH

The element valences and elemental compositions (Table S1) in Mn/Mg/Fe-LDH were explored through the corresponding XPS data. The high-resolution scans of core-level photoelectron spectrum (C 1s, O 1s, N 1s, Mg 1s, Fe 2p, and Mn 2p) are explored.

The XPS spectrum of C 1s (Figure S5) for Mn/Mg/Fe-LDH showed two peaks of binding energy (BE) at 284.30 eV and 287.98 eV attributed to the C–C bond in adventitious carbon (Mubarak et al., 2018) and the C=O bond in the host CO_3^{2-} anion in its interlayer region (Huang et al., 2015; Liu et al., 2019), respectively. The presence of another important host NO_3^- anion in this interlayer region was confirmed through N=O bond at 407.03 eV in the N 1s XPS spectrum (Figure S6) or Table S1 (Goh et al., 2009). The CO_3^{2-} ions generated by CO_2 from atmosphere into the interlayer region during the synthesis of Mn/Mg/Fe-LDH (Section 2.2) (Mubarak et al., 2018); meanwhile, NO_3^- ions were derived from the metal salts of Mg, Fe, and Mn used (Section 2.1). The presence of C and N elements, which was obtained from EDS data (Figure S3) and XPS data (Table S1), and visible in mapping pictures (Figure S4), might result from the $CO_3^{2-}$and NO_3^- anions in its interlayer region. The host CO_3^{2-} and NO_3^- anions have been acknowledged as active anions for efficiently exchanging hexavalent chromium anions (CrO_4^{2-} and $Cr_2O_7^{2-}$) (Tran et al., 2019; Varga et al., 2021) and arsenate anions ($H_2AsO_4^-$ and $HAsO_4^{2-}$) (Yu et al., 2012; Lee et al., 2018) from water environments.

The high-resolution O 1s spectrum (Figure 4a or Figure S7) can be divided into three distinct peaks. Two BE peaks at 529.05 and 530.97 eV correspond to the M–O–M (or M–O where M represents for Mg, Mn, or Fe) and M–O–H (hydroxyl group). Another peak at 532.52 eV is the overlap of the M–O–H^+_2 (protonated hydroxyl group), H–O–H (water molecule), and C=O (carbonate) bonds (Goh et al., 2009; Iruretagoyena Ferrer, 2016; Hudcová et al., 2017; Penke et al., 2021; Wang et al., 2021; Zhang et al., 2022).

For magnesium, the BE value at 1303.3 eV (the XPS spectrum of Mg 1s in Figure S8) is related to the form of hydroxide of $Mg(OH)_2$ in Mn/Mg/Fe-LDH. In contrast, Fe and Mn that are transition metals, so they can change their oxidation states under suitable conditions. Thus, it is necessary to consider both their raw XPS spectra and deconvoluted XPS spectra.

The raw spectrum of Mn 2p (Figure S9) indicated two BE peaks at 641.29 eV (Mn $2p_{3/2}$) and 652.91 eV (Mn $2p_{1/2}$), which implies the existence of the dominant Mn^{3+} oxidation state in Mn/Mg/Fe-LDH (Guo et al., 2016; Zhang et al., 2022). Although the $Mn(NO_3)_2$ salt used for preparing Mn/Mg/Fe-LDH, under high alkaline aqueous condition at pH 12 (Section 2.2), Mn^{2+} was easily oxidized to Mn^{3+}. This is because such reaction (Equation 3) occurs with a low standard reduction potential (E^{o}_{red}) (Haynes, 2010; Guo et al., 2016). However, highly unstable Mn^{3+} can continue to be oxidized to Mn^{4+} (Zhang et al., 2022). Many other authors reported a similar oxidation phenomenon when preparing LDH solids (Guo et al., 2016; Zhou et al., 2021; Zhang et al., 2022). For example, Zhang et al. (2022) prepared Ni/Mn-LDH from $Ni(NO3)_2$ and $MnSO_4$. The XPS spectrum indicated the attribution of Mn^{3+} at 641.75 eV (Mn $2p_{3/2}$) and 652.60 eV (Mn $2p_{1/2}$).

$$Mn(OH)_3 + e^- \rightleftharpoons Mn(OH)_2 + OH^- \qquad (E^{o}_{red} = 0.15\ V) \qquad (3)$$

To verify the oxidation state of Mn in Mn/Mg/Fe-LDH, the narrowed scan of Mn $2p_{3/2}$ was applied based on the recommendations of previous studies (Figure 5a or Figure S10a). The oxidation states of Mn^{2+} [in the form of $Mn(OH)_2$ solid], Mn^{3+} [in $Mn(OH)_3$ solid], and Mn^{4+} [in MnO_2 solid] were observed at the corresponding BE peaks at 640.08, 641.35, and 642.55 eV, respectively (Mohammadi et al., 2021; Zhou et al., 2021). The percentages of Mn^{2+}, Mn^{3+}, Mn^{4+} in Mn/Mg/Fe-LDH that were calculated based on the area of the corresponding peaks in the core level spectrum of the Mn $2p_{3/2}$ region were 27.52%, 42.28%, and 30.20%, respectively. Similarly, Zhou et al. (2021) concluded that Ni/Mn-LDH contained 57% for Mn^{3+} and 43% for the others (Mn^{2+} and Mn^{4+}) based on the Mn $2p_{3/2}$ data.

The raw XPS spectrum of Fe 2p indicated two BE peaks at 711.02 and 724.38 eV (Figure S11). Those peaks are typical characteristics for the Fe^{3+} oxidation state in some LDH materials such as Co/Fe-LDH (Wang et al., 2021), Mg/Fe-LDH (Mubarak et al., 2018), and Mg/Zn/Fe (Liu et al., 2019). The high-resolution Fe 2p XPS spectrum was deconvoluted into four peaks (Figure 5b or Figure S12a). The result of the detail deconvolution suggested that both Fe^{3+} (52.84%) and Fe^{2+} (47.16%) coexisted in Mn/Mg/Fe-LDH. Similarly, Wang et al. (2021) prepared Co/Fe-LDH from two salts ($CoCl_2$ and $FeCl_3$) and concluded the coexistence of Fe^{3+} and Fe^{2+} in Co/Fe-LDH (based on their XPS data). A similar conclusion was reported by other scholars (Mubarak et al., 2018) for Mg/Fe-LDH. They found that the Fe^{3+}/Fe^{2+} ratio in Mg/Fe-LDH that was obtained based on the relative areas of the Gaussian peaks in the Fe 2p XPS spectrum was 0.34/1 (Mubarak et al., 2018). The presence of Fe^{2+} in Mn/Mg/Fe-LDH might result from some reduction reactions (Equation 4 and Equation 5) (Haynes, 2010).

$$Fe(OH)_3 + e^- \rightleftharpoons Fe(OH)_2 + OH^- \qquad (E^o_{red} = -0.56\ V) \tag{4}$$

$$Fe^{3+} + e^- \rightleftharpoons Fe^{2+} \qquad (E^o_{red} = 0.15\ V) \tag{5}$$

In essence, a reduction–oxidation (redox) reaction is spontaneous if the standard electrode potential for this reaction (E^o_{redox}) is positive, and vice versa. Possible redox reactions between Mn^{2+} and Fe^{3+} are expressed as Equation 6 and 7 (Haynes, 2010). Considering the sign of E^o_{redox}, it can be concluded that the redox reaction (Equation 7) occurred spontaneously during the synthesis process of Mn/Mg/Fe-LDH.

$$Mn(OH)_2 + Fe(OH)_3 \rightleftharpoons\ Mn(OH)_3 + Fe(OH)_2 \qquad (E^o_{redox} = -0.71\ V) \tag{6}$$

$$Mn(OH)_2 + Fe^{3+} + OH^- \rightleftharpoons\ Mn(OH)_3 + Fe^{2+} \qquad (E^o_{redox} = 0.621\ V) \tag{7}$$

3.2.5. Electrical state of the surface of Mn/Mg/Fe-LDH solution

The change in the external surface charge of Mn/Mg/Fe-LDH with changing solution pH is defined by its pH_{IEP}. Figure 6a shows that the Mn/Mg/Fe-LDH material had a high pH_{IEP} of 10.15 ± 0.06, which is similar to earlier studies done with Mg/Al-LDH (pH_{IEP}= 10.9) (Li et al., 2009), *in-situ* synthesized Mg/Al-LDH (pH_{IEP} = 11.5) (Chao et al., 2018), and Mg/Fe-LDO (pH_{IEP} > 12; its zeta potential at pH 12 = 8.67 mV) (Mubarak et al., 2018). In addition, Chubar et al. (2013) reported that the pH_{IEP} value of Mg/Al-LDH ($pH_{IEP} \approx 9.7$) was not affected by the preparation methods (i.e., alkoxide sol–gel method, alkoxide-free sol–gel synthesis, and hydrothermal precipitation). The outcome suggested that Mn/Mg/Fe-LDH exhibited a positive charge on its external surface with solution pH values lower than its pH_{IEP} (Figure 6a). This is because of the protonation of abundant –OH groups (its p*K*a ranging from 9.0 to 10) on its external surface (Jiao and Hou, 2007; Li et al., 2009; Tran et al., 2019). Therefore, it is expected that As(V) anions can be effectively removed from solution by the $–OH_2^+$ groups on the external surface of Mn/Mg/Fe-LDH (also known as electrostatic attraction).

3.3. Effect of solution pH on the adsorption process

The effect of different initial solutions pH (2.0–10) on removal efficiency of As(III) and As(V) by Mn/Mg/Fe-LDH for two initial arsenic concentrations (i.e., 3.5 and 55 mg/L) is presented in Figure 6b. At initial arsenic concentration (C_o) of ~3.5 mg/L, the removal efficiency of As(III) and As(V) using Mn/Mg/Fe-LDH is nearly similar because Mn/Mg/Fe-LDH exhibited a very high affinity to the arsenic contaminants. An analogous result was reported by Wang and co-workers (2021) for adsorption of As(III) and As(V) at different C_o values (i.e., 5, 10, and 50 mg/L) onto Fe/Mn-C-LDH. Consequently, the influence of different solutions pH on the adsorption process was not clear in a low initial arsenic concentration scenario.

Figure 6b shows that the adsorption capacity of Mn/Mg/Fe-LDH at very high initial arsenic concentration (~55 mg/L) dramatically decreased when the solution pH increased from 2.0 to 10. A similar tendency was found for the As(III) and As(V) adsorption onto Mn/Fe-LDH (Otgonjargal et al., 2012), Mg/Fe-LDH (Hong et al., 2014), and α-alanine-intercalated Mg/Fe-LDH (Hong et al., 2014). Under strong acidic conditions (i.e., pH 2.0), the structure of Mn/Mg/Fe-LDH might not be stable (Wang et al., 2021) because it was synthesized through the co-precipitation method at pH 12 (see Section 2.2). This means that the components (Fe, Mg, and Mn) in its structure were released into the solution (Table 1).

The released Fe ions might then react with As(III) and As(V) in solution to form precipitates such as $FeAsO_4 \bullet 2H_2O$ (Lenoble et al., 2005), $Fe_3(AsO_4)_2 \bullet 8H_2O$ (Lenoble et al., 2005), and amorphous ferric arsenate (Tian et al., 2017). In addition, the concentrations of Fe after adsorption of As(III) (0.071 mg/L) and As(V) (0.045 mg/L) were significantly lower than that of the blank sample (11.25 mg/L; Table 1), confirming the existence of certain reactions (possible co-precipitation) between Fe and As.

To evaluate the feasibility of reaction between the leached metals and As ions in solution, adsorption and removal studies of As ions from solutions were carried out at pH 2.0. The concentrations of the leached metals were prepared based on the result in Table 1. The results (Table S2) showed that a presence of certain reaction between Fe ions and As ions in solution. However, the removal efficiency of As by the metal ions from water was remarkably lower than using the Mn/Mg/Fe-LDH material. For example, the percentages of As(III) and As(V) ions in solution removed by the percentages of Fe^{3+} ions were only 9.17% and 5.16%, respectively. In contrast, the corresponding removal efficacies of As(III) and As(V) by the Mn/Mg/Fe-LDH solid were 80% and 84.8%, respectively (Table S2). The result suggested that reactions between the leached metals and As ions in solution at pH 2.0 were not a main removal mechanism. In addition, the mass loss of Mn/Mg/Fe-LDH (calculated by the dry mass) after adsorption at pH 2.0 was only around 5%. This means that the amounts of the metals leached

from Mn/Mg/Fe-LDH were not enough to remove effectively As ions from water. Therefore, the highest removal percentage of As(III) or As(V) by Mn/Mg/Fe-LDH (Figure 6b) at pH 2.0 mainly resulted from the adsorption mechanism of As ions in solution onto the material. In fact, Figure 6a shows that Mn/Mg/Fe-LDH exhibited the highest positive value of zeta potentials (+45.2 mV; Figure 6a) at pH 2.0. As a result, electrostatic attraction between the positively charged surface of Mn/Mg/Fe-LDH and As(V) anions in solutions played a critical role in adsorption mechanism.

Although at solution pH 2.0, the removal efficiency was the highest, the structure of Mn/Mg/Fe-LDH was relatively less stable. As well, the removal mechanism was the combination of adsorption and other chemical reactions (i.e., precipitation). For a real-life application the solution pH value often ranges from 6.0 to 8.0 (especially for groundwater; Section 3.13). Therefore, the subsequent study was conducted with an initial solution pH of 7.0.

3.4. Effect of foreign anions on the adsorption process of As(III) and As(V)

The (inhibitory) effect of the presence of foreign anions on the As removal process was explored by using five anions (Cl^-, SO_4^{2-}, CO_3^{2-}, SiO_3^{2-}, and HPO_4^{2-}) at two initial concentrations (10 mM and 100 mM). Results indicated that the strong competition between foreign anions and As ions in aqueous solution led to a remarkable decline in the efficiency of removing As(III) and As(V) (Figure 7).

In general, the adsorption capacity of Mn/Mg/Fe-LDH followed the order of no competition (absence of foreign anions) > chloride (the presence of Cl^- anion) > sulphate (SO_4^{2-}) > phosphate (HPO_4^{2-}) > carbonate (CO_3^{2-}) > silicate (SiO_3^{2-}) > five foreign anions (Cl^-, SO_4^{2-}, CO_3^{2-}, SiO_3^{2-}, and HPO_4^{2-}). An identical adsorption tendency has been reported in the literature (Hong et al., 2014; Lu et al., 2018).

Among coexisting single anions, the presence of Cl^- anions had the lowest inhibitory effect on the removal efficiency of As ions by Mn/Mg/Fe-LDH. This is because chloride is

monovalent anion with its lower ionic charge density than As(V) anions and lacks tetrahedral structure. In contrast, SiO_3^{2-} and CO_3^{2-} were the strongest competing anions. As discussed in Section 3.2, CO_3^{2-} was the host anions in the interlayer region of Mn/Mg/Fe-LDH; therefore, it was more favourable to this region than guest As(V) anions. In addition, SiO_3^{2-} and CO_3^{2-} exhibited a similarity in their structure and chemical behaviour because they are the same group in the periodic table. Therefore, SiO_3^{2-} and CO_3^{2-} had a stronger competitive adsorption than As(V) anions in the interlayer region. For competitor anion (HPO_4^{2-}), phosphate and arsenate exhibit similar tetrahedral structures and are listed in the same group in the periodic table (Hong et al., 2014; Lu et al., 2018). Therefore, they have the same adsorption competition to the exchange sites in the interlayer region of Mn/Mg/Fe-LDH (Lu et al., 2018).

The results suggested an integral role of anion exchange in the adsorption process of arsenic ions onto the interlayer region of Mn/Mg/Fe-LDH. As(V) anions in solution are easily exchanged with the host anions in the interlayer region of Mn/Mg/Fe-LDH. In contrast, As(III) ions might be firstly oxidized into As(V) anions. Subsequently, oxidized As(V) anions were exchanged with the host anions present in the Mn/Mg/Fe-LDH material.

3.5. Adsorption kinetics

The adsorption kinetics results are provided in Figure S13**.** The reaction between the Mn/Mg/Fe-LDH and the adsorbate [As(III) or As(V)] remarkably increased within the first contact period of 60 min, and then it proceeded at a relatively slower rate before achieving equilibrium at approximately 20 h. Other scholars also reported that the adsorption process of arsenic ions [As(III) and As(V)] onto Mn/Fe-LDH and *α*-alanine intercalated Mg/Fe-LDH reached an equilibrium within 30 h (Otgonjargal et al., 2012) and 24 h (Hong et al., 2014), respectively. In this work, four common kinetic models, namely pseudo-first-order (PFO), pseudo-second-order, Avrami, and Elovich models were applied to describe the experimental data of adsorption with time. The relevant information concerning the non-linearized form of those models is given in Section S2 (Supporting information).

Table S3 provides the values of kinetic parameters of the selected kinetic models. On the basis of the statistics (R^2 and χ^2), the Avrami and Elovich models described the experimental data of time-dependent adsorption (adsorption kinetics) better than the PSO and PFO models. The adsorption rate constant (k_{AV}) of the Avrami model indicated that the adsorption process of As(III) (0.013/min) onto LDH was faster than that of As(V) (0.003/min). A similar conclusion was reported by Wang et a. (2021). However, at the beginning the adsorption process of As(V) occurred more rapidly than that of As(III) because the initial adsorption rate (α) of As(V) adsorption [707 mg/(g×min)] was overwhelmingly higher than that of As(III) one [378 mg/(g×min)]. This might be because As(III) ions in solution were oxidized into As(V) when they came into contact with the LDH material first. Subsequently, the oxidized As(V) ions and As(III) ions in solution were removed from solution (i.e., adsorbed onto LDH).

3.6. Adsorption isotherm

Adsorption isotherms for As(V) and As(III) by Mn/Mg/Fe-LDH at different solution temperatures is provided in Figure 8. The isotherms are categorized as H-shape (Lyklema, 1995). Therefore, Mn/Mg/Fe-LDH can effectively remove both As(V) and As(III) from water even at small initial concentrations. Yang et al. (2005) also reported that calcined and uncalcined LDH materials can eliminate efficiently arsenic ions (trace levels) from aqueous water under the trace levels. Five adsorption isotherm models are applied to describe the experimental data of adsorption equilibrium. They (the Langmuir, Freundlich, Langmuir–Freundlich, Redlich–Peterson, and Khan models) are introduced in Section S3 (Supporting information).

According to higher R^2 and lower χ^2 (Table 2), the three-parameter models of adsorption isotherm (i.e., the Langmuir–Freundlich, Redlich–Peterson, and Khan models) fitted well to the experimental data of adsorption equilibrium compared to the two-parameter models (Langmuir and Freundlich). Although the parameters (Q_{LF}, Q_{Khan}, and Q^o_{max}) of the models (Langmuir–Freundlich, Khan, and Langmuir, respectively) can provide information on the maximum

adsorption capacity of LDH to As(III) and As(V), the parameter Q^{o}_{max} of the Langmuir model is more consistent with the experimental data in Figure 8. In fact, the adsorption capacity of As(V) and As(III) onto Mn/Mg/Fe-LDH at 25 °C was higher than at 50 °C and 7 °C (Figure 8). Therefore, the values of Q_{LF}, Q_{Khan}, and Q^{o}_{max} should follow the order of 25 °C > 50 °C > 7 °C to be consistent with the experimental data in Figure 8. However, the Q_{LF} value followed the decreasing order: 25 °C > 7 °C > 50 °C, while the Q_{Khan} follows the order of 50 °C > 25 °C > 7 °C for the As(V) adsorption. Therefore, the adsorption capacity of Mn/Mg/Fe-LDH towards As(III) and As(V) was reflected through the Q^{o}_{max} of the Langmuir model. Thus, the parameter Q^{o}_{max} is used for discussion and comparison.

As shown in Table 2, Mn/Mg/Fe-LDH exhibited a higher affinity of As(III) than As(V) in solution. For example, the Q^{o}_{max} value for As(V) adsorption (56.1 mg/g) by Mn/Mg/Fe-LDH at 25 °C was higher than that for As(III) adsorption (32.2 mg/g). This means that Mn/Mg/Fe-LDH exhibited a high affinity for As(III) compared to As(V). This finding was similar to that of other researchers (Hong et al., 2014; Kong et al., 2014; Bai et al., 2016; Guo et al., 2017; Wang et al., 2021) on the adsorption of As(III) and As(V) onto some similar LDH-based materials. However, an opposite tendency was reported by Choong et al. (2021) using Mg/Fe-LDH embedded by polyacrylamide and polyvinyl alcohol and Bagherifam et al. (2014) using SO_4-intercalated Zn/Al-LDH. If anion exchange plays an important role in the adsorption process, the amount of As(V) anions adsorbed by Mn/Mg/Fe-LDH (exchanged with the host anions in its interlayer region) would have been higher than that of As(III) ions. This is because As(III) might be partly oxidized into As(V) but not totally. Therefore, it was evident that other dominant adsorption mechanisms (i.e., inner-sphere complexation) existed, not just anion exchange in adsorbing As(III) onto Mn/Mg/Fe-LDH.

The maximum adsorption capacity of Mn/Mg/Fe-LDH to As(III) and As(V) ions is compared to some other materials investigated in the literature (Table S4). As expected, the prepared Mn/Mg/Fe-LDH material (Q^{o}_{max} = 56.1 mg/g) exhibited higher adsorption capacity of

toxic As(III) ions than others such as the composite of Fe/Mn-LDH and carbon (36.1 mg/g) (Wang et al., 2021), Zn/Al-LDH (34.2 mg/g) (Bagherifam et al., 2014), aluminum-enriched biochar prepared from Tetra paks (24.2 mg/g) (Ding et al., 2018), alumina composite modified activated carbon (14.3 mg/g) (Karmacharya et al., 2016), tire rubber alumina composite (13.51 mg/g) (Karmacharya et al., 2016), Fe/Mn modified biochar (8.25 mg/g) (Lin et al., 2017), and natural laterite (0.51 mg/g) (Nguyen et al., 2020).

Furthermore, under the same experimental conditions (i.e., ~50 mg/L, 30 °C, pH = 7.0, 1.0 g/L, 24h), the adsorption capacity of Mn/Mg/Fe-LDH towards As(III) and As(V) ions (21.3 and 11.2 mg/g; Figure S14) exceeded commercial activated carbon (0.205 and 0.309 mg/g, respectively). Therefore, it can be concluded that Mn/Mg/Fe-LDH was a promising material for the remediation of arsenic-contaminated water.

3.7. Adsorption thermodynamics

The effect of solution temperatures on the adsorption process was investigated at 7 °C, 25 °C, and 50 °C (Figure 8). Results indicated that an increase in temperature from 7 °C to 25 °C increased the amounts of As(V) and As(III) removed from solution (adsorbed onto LDH). However, a further rise to 50 °C caused a significant reduction in the amount of As(V) and As(III) removed. This might be due to the desorption phenomena occurring at the high temperature of 50 °C.

The thermodynamic parameters ($\Delta G°$, $\Delta H°$, and $\Delta S°$) of the arsenic adsorption by Mn/Mg/Fe-LDH are computed using the van't Hoff equation. The standard free energy change ($\Delta G°$) is directly calculated from Equation 8:

$$\Delta G° = -RT \ln K^{o}_{\text{Equilibrium}} \quad (8)$$

The relationship among the three thermodynamic parameters ($\Delta G°$, $\Delta H°$, and $\Delta S°$) is provided in Equation 9:

$$\Delta G° = \Delta H° - T\Delta S° \quad (9)$$

The van't Hoff equation (Equation 10) is obtained by substituting Equation 8 for Equation 9:

$$\mathrm{Ln}K^{\mathrm{o}}_{\mathrm{Equilibrium}} = \left(\frac{-\Delta H°}{R}\right) \times \frac{1}{T} + \frac{\Delta S°}{R} \quad (10)$$

$$K^{\mathrm{o}}_{\mathrm{Equilibrium}} = \frac{K_{\mathrm{model}}(\mathrm{L/mol}) \times C^{\mathrm{o}}(\mathrm{mol/L})}{\gamma} \quad (11)$$

where K_{model} (L/mol) is the Langmuir constant (K_{L}), the Langmuir–Freundlich constant (K_{LF}), or the Khan constant (K_{Khan}); $K^{\mathrm{o}}_{\mathrm{Equilibrium}}$ (dimensionless) is thermodynamic equilibrium constant; $C°$ is the selected standard state of arsenic ($C°$ = 1 mol/L); T is temperature (K); R is a gas constant [0.00831 kJ/(mol×K)]; and γ is an activity coefficient of arsenic in solution.

Table S5 shows the thermodynamics parameters for the adsorption process (7 °C, 25 °C, and 50° C) obtained based on the equilibrium constant of the adsorption isotherm models (K_{L}, K_{LF}, and K_{Khan}). Because the R^2 value of the van't Hoff equation is very low (Table S5), the $\Delta H°$ and $\Delta S°$ parameters cannot be obtained for whole adsorption process. Table 3 provides the thermodynamics parameters calculated at two ranges of temperatures: 7 °C and 25 °C (280–298 K); and 25 °C and 50 °C (298–323 K). Of the three equilibrium constants, only the Langmuir constant K_{L} is suitable for application as $K_{\mathrm{Equilibrium}}$ because the sign of $\Delta H°$ is consistent with the experimental data depicted in Figure 8. For example, the adsorption capacity of Mn/Mg/Fe-LDH towards As(V) and As(III) decreased when temperature increased from 25 °C to 50 °C; therefore, $\Delta H°$ must be negative. In this study, standard enthalpy change ($\Delta H°$) was calculated for each two-temperature using Equation 12, and standard entropy change ($\Delta S°$) was computed from Equation 12.

$$\Delta H° = R\left(\frac{T_2 \times T_1}{T_2 - T_1}\right) \ln\left(\frac{K_{T_2}}{K_{T_1}}\right) \quad (12)$$

where T_2 and T_1 are the two operation temperatures ($T_2 > T_1$); and $K_{\mathrm{T_1}}$ and $K_{\mathrm{T_2}}$ are the equilibrium constants ($K^{\mathrm{o}}_{\mathrm{Equilibrium}}$) at T_2 and T_1, respectively.

The results (Table S5) indicated that the adsorption process of arsenic ions by Mn/Mg/Fe-LDH occurred spontaneously because of the negative values of $-\Delta G°$ (calculated based on the Langmuir constant, for example, $\Delta G°$ for: As(V) adsorption (–19.7 kJ/mol at 280 K, –22.9 kJ/mol at 298 K, and –23.8 at 323 K); and As(III) adsorption (–20.1 kJ/mol at 280 K, –22.7 kJ/mol at 298 K, and –23.8 at 323 K).

As shown in Table 3, the adsorption process of As(V) onto Mn/Mg/Fe-LDH was endothermic within the 280–298 K temperature range ($\Delta H°$ = +29.9 kJ/mol) and exothermic within 298 K and 323 K ($\Delta H°$ = –11.4 kJ/mol). A similar tendency was observed for As(V) adsorption that was $\Delta H°$ = +19.3 kJ/mol (280–298 K) and $\Delta H°$ = –8.75 kJ/mol (298–323K). Furthermore, the positive values of $\Delta S°$ suggest that the organization of arsenic at the solid/liquid interface during the process of As(III) and As(V) adsorption become more random. A positive value of $\Delta S°$ was reported for the adsorption of As(III) and As(V) onto Mn/Fe-LDH (Otgonjargal et al., 2012).

3.8. Desorption study

Different solvents (Na_2CO_3, NaCl, EDTA, NaOH, deionized water adjusted to pH 12, and HCl) were used to examine the desorption efficiency of As from the laden Mn/Mg/Fe-LDH. The result demonstrated that the desorption efficiency of both As(III) and As(V) was negligible (lower than 1.0%) for all desorbing agents used (Table S6), suggesting that the adsorption was highly irreversible. Subsequently, reusing Mn/Mg/Fe-LDH samples after adsorption was not feasible. In contrast, Goh et al. (2009) found that the adsorption process of As(VI) by nitrate-intercalated Mg/Al-LDH was reversible, with the desorption efficiency being 68.3% or 76.6% (using 0.1 M NaOH or Na_2CO_3, respectively). High desorption efficiency resulted from the reversible adsorption mechanism of As(VI) and anion the Mg/Al-LDH that was anion exchange between As(VI) anions and the host NO_3^- in its interlayer region (Goh et al., 2009).

3.9. Leaching test after the adsorption process

The stability of synthesized Mn/Mg/Fe-LDH at different pH solutions was evaluated through the leaching test. Because the pH value of drinking water often ranges from 6.0 to 8.0, the data obtained from this pH range were used for discussion. **Table 1**'s results show that the amount of Fe and Mn leached from Mn/Mg/Fe-LDH after adsorption of As(V) and As(III) was smaller than that established by the Vietnamese government's national technical regulation on drinking water quality (<0.3 mg/L for total Fe or Mn). Magnesium ions are necessary for good human health. However, too high a level of Mg (10–100 mg/L) in drinking water can pose serious health risks such as heart disease (Rosanoff, 2013). The Mg concentrations after the adsorption process ranged from 1.79 to 3.98 mg/L. Therefore, the concentrations of Mg, Mn, Fe ions leached from the Mn/Mg/Fe-LDH after adsorption are in the safe range limit for drinking water.

3.10. Possible adsorption mechanism of adsorption mechanism of soluble As(V) oxyanions

The adsorption mechanism of As(V) oxyanions by Mn/Mg/Fe-LDH was discussed at pH 7.0 and illustrated in Figure 10. Under neutral pH, inorganic As(V) species exist as predominantly monovalent $H_2As^VO_4^-$ anion and divalent $HAs^VO_4^{2-}$ anion (Figure S1).

3.10.1. Reduction of As(V) to As(III) by Mn/Mg/Fe-LDH

An important question is whether (1) As(V) is reduced into As(III) by LDH-based materials and (2) the As(V) and reduced As(III) ions are adsorbed onto the materials. To confirm the reduction phenomenon, the speciation of As present in the As(V)-laden LDH materials is confirmed by relevant techniques: X-ray absorption near edge structure (XANES) and XPS. It is hypothesized that the presence of As(V) in the LDH materials does not destroy their unique layer structure. This means that the XRD patterns of LDH solids before and after adsorption of As(V) are nearly the same (the original layer structure of LDH is preserved). In this case, the (003) plane is still detected in the As(V)-laden LDH samples.

For example, Wang et al. (2021) applied XPS to identify the reduction process of As(V) by the composite of Fe/Mn-LDH and bamboo carbon. They found that only As(V) speciation existed in the composite. The As 3d spectrum of the laden composite indicated one peak at 44.32 eV. The original layer structure of the material (XRD data) was still maintained after adsorption (Figure S15b). The results suggested that As(V) was not reduced to As(III) during the adsorption process. A similar conclusion was obtained for adsorption As(V) by Mg/Fe-LDH (Hudcová et al., 2017), Mg/Al-LDH (Huang et al., 2015), Cl-intercalated Mg/Fe-LDH (Guo et al., 2017), NO_3-intercalated Mg/Al-LDH (Goh et al., 2009), Mg/Fe-LDH embedded with polymers (Choong et al., 2021), and SO_4-intercalated Zn/Al-LDH (Bagherifam et al., 2014).

Similarly, Wang et al. (2009) applied XANES to identify this reduction process. Their results on the comparison on XANES spectra of As(III) standard, As(V) standard, and As(V)-laden Mg/Al-LDH indicated that As(V) was not reduced into As(III) following the process of As(V) adsorption by Mg/Al-LDH. An analogous conclusion was reported by some researchers who used XANES to identify the reduction process of As(V) by Li/Al-LDH (Liu et al., 2006) and by Guo Cl-intercalated Mg/Fe-LDH (Guo et al., 2017).

However, the reduction of As(V) to As(III) after the equilibrium adsorption was identified in this study through the XPS data. In essence, the binding energy (BE) of As(V) is higher than that of As(III). For example, the BE value of As(III) derived from the pure chemical $NaAsO_2$ was 44.2 eV (Bang et al., 2005), while the corresponding value for As(V) from $Na_2HAsO_4{\bullet}7H_2O$ was 45.6 eV (Soma et al., 1994). Figure 9a shows that the dominant arsenic species in Mn/Mg/Fe-LDH was As(III), with the BE value in the low resolution XPS survey being 44.17 eV (Table S1). The deconvoluted result of the high resolution of As 3d spectrum (Figure 9d) showed that after adsorption As(V), the percentage of As(III) species (64.02%) in Mn/Mg/Fe-LDH dominated than that of As(V) species (35.98%). In addition, previous study reported the photoelectron peak for As(0) was at 41.4 eV (Figure S16) (Bang et al., 2005). However, there was not existence of As(0) species in the laden Mn/Mg/Fe-LDH (Figure 9d).

577 The results suggested that As(V) was only reduced to As(III) when As(V) in solutions contacted
578 with Mn/Mg/Fe-LDH. The reduction mechanism of inorganic As(V) species to As(III) species
579 might be expressed as Equations 13–14 (Bang et al., 2005). As(V) and reduced As(III) were
580 adsorbed by Mn/Mg/Fe-LDH through some below mechanisms.

$$H_2AsO_4^- + 2Fe^{2+} + 3H^+ \rightleftharpoons H_3AsO_3^0 + 2Fe^{3+} + H_2O \quad (13)$$

$$HAsO_4^{2-} + 2Fe^{2+} + 4H^+ \rightleftharpoons H_3AsO_3^0 + 2Fe^{3+} + H_2O \quad (14)$$

581 ***3.10.2. Dissolution–precipitation mechanism***

582 Some authors reported that reactions between Fe-containing materials (i.e., ferrihydrite)
583 and As(V) (prepared from Na_3AsO_4•$12H_2O$) can generate a scorodite ($FeAsO_4$•$2H_2O$ and its
584 p*K*a = 20.24) (Frau et al., 2010). They authors reported that the BE of As(V) in the scorodite
585 (the As 2p spectrum) was approximately 46 eV (Frau et al., 2010). Furthermore, based on the
586 XRD data of the carbonate structural Fe(II) material (CSF) before and after adsorption of
587 As(V), Tian et al. (2017) concluded that the existence of adsorption mechanism involved in
588 surface precipitation. Their XRD data (Figure S17) confirmed the formation of the crystalline
589 parasymplesite ($Fe_3(AsO_4)_2$•$8H_2O$ and its p*K*a = 33.25) on the As(V)-laden material (Tian et
590 al., 2017). This reaction between Fe^{2+} and As(V) (from NaH_2AsO_4) in solutions to form the
591 precipitation of ferrous arsenate is expressed as Equation 15 (Johnston and Singer, 2007).

$$2HAsO_4^{2-} + 3Fe^{2+} = Fe_3(AsO_4)_2 + 2H^+ \quad (15)$$

592 Furthermore, Tournassat et al. (2002) investigated the adsorption of As(III) by birnessite
593 (MnO_2•nH_2O). They found that As(III) was oxidized to As(V) by birnessite. The oxidized
594 As(V) reacted to Mn^{2+} ions (released from birnessite) through the krautite reaction to form the
595 precipitation of manganese(II) arsenate ($MnHAsO_4$•H_2O; Equation 16) (Tournassat et al.,
596 2002).

$$H_2AsO_4^- + Mn^{2+} + H_2O = MnHAsO_4 \bullet H_2O + H^+ \quad (16)$$

Guo et al. (2017) studied the adsorption of As(V) or As(III) by Cl-intercalated Mg/Fe-LDH. The presence of precipitates of hornesite ($Mg_3(AsO_4)_2 \cdot 8H_2O$) or ($Fe_4(AsO_4)_2O_3$) in the As(V)-laden LDH solid was identified by XRD at a peak of ~30°. However, the relevant peak at around 30° was not observed in the As(II) laden LDH material.

However, the leaching test indicated that the structure of Mn/Mg/Fe-LDH was highly stable under pH 7.0 (Table 1). The reactions between the dissolved metals (i.e., Mg, Fe, and Mn) from Mn/Mg/Fe-LDH and As(V) in solution had a minor contribution to the removal efficiency of As(V) (Section 3.3). Therefore, the dissolution–precipitation mechanism was less important (or possibly ruled out) in this study. The conclusion was supported by the XRD data of Mn/Mg/Fe-LDH before and after adsorption (Figure 1) and the XPS data (Figure 9). An analogous conclusion was stated by many researchers (Wang et al., 2009; Guo et al., 2017; Choong et al., 2021; Wang et al., 2021).

3.10.3. Outer-sphere and inner-sphere complexations

The out-sphere surface complex (also known as weak electrostatic attraction) that occurred between the positively charged surface of Mn/Mg/Fe-LDH and As(V) anions in solution was highly expected as a primary adsorption mechanism of As(V) anions (Wang et al., 2009; Choong et al., 2021). This interaction was supported by the positively charged surface of Mn/Mg/Fe-LDH confirmed by its zeta potentials (Figure 6a). In contrast, the XPS and FTIR techniques did not give a reliable information on this weak interaction. A similar identification on this mechanism has reported by other scholars for studying the adsorption of As(V) anions onto some materials with similar properties (Tian et al., 2017). However, this attraction (weak and reversible) might only exist in the first period of the adsorption process. This conclusion was confirmed by the desorption study (Section 3.8). After the 24h-equilirum adsorption, the presence of As ions in the laden Mn/Mg/Fe-LDH material was very strong. This might be because As(V) anions were reduced to As(III) ions, and the reduced As(III) ions were strongly

adsorbed by Mn/Mg/Fe-LDH through stronger interactions (or irreversible adsorption mechanism). Therefore, the desorption efficiency was negligible (only 0.5%; Table S6).

With regard to inner-sphere complex, Wang et al. (2009) found that As(V) can react with the oxygen-containing functional groups of Mg/Al-LDH (mainly –OH groups on its surface) through this complexation. The dominant inner-sphere complexation through ligand exchange was confirmed by Arsenic K-edge XAS (X-ray absorption spectroscopy) spectrum. Figure 4 shows that after adsorption of As(V), the intensity of the BE peak at approximately 533 eV (M–OH_2^+) decreased, but that at around 529 eV (M–O–M) increased (Figure S7). The changes of relevant peak intensities in the O 1s spectrum after the 48h-adsorption of As(V) suggested the existence of inner-sphere complexation between As(V) oxyanions or reduced As(III) ions and the hydroxyl groups on the surface of LDH. The different kinds of inner-sphere surface complexes of arsenic summarized in Figure S18 (Wang and Mulligan, 2008). This complexation was found in the adsorption process of As(V) and As(III) using LDH-based materials (Liu et al., 2006, 2006; Goh et al., 2009; Wang et al., 2009; Liu et al., 2019; Choong et al., 2021) and others (Liu et al., 2006; Penke et al., 2021).

3.10.4. Anion exchange

In general, LDH contains abundant host anions (i.e., NO_3^- and CO_3^{2-}), so anion exchange between As(V) anions in solution and its host anions in the interlayer region is highly feasible (Goh et al., 2009; Huang et al., 2015; Asiabi et al., 2017; Hudcová et al., 2017). This conclusion was confirmed by the results of competitive adsorption of foreign anions (Figure 7). The adsorption capacity of Mn/Mg/Fe-LDH (Figure 7) declined remarkably due to the presence of foreign anions in solution (competitive adsorption). For example, it fell from 14.5 mg/g (no competition) to approximately 1.5 mg/g (competition between arsenate and phosphate anions for exchangeable sites in Mn/Mg/Fe-LDH). Some other techniques were also helpful to identity this mechanism, such as FTIR (Figure 3), XRD (Figure 1), and XPS (Figures S5–S6).

The FTIR data (Figure 3) showed that the intensity of the bands at around 1348 cm^{-1} (N=O in NO_3^- overlapped C=O in CO_3^{2-}) decreased markedly after adsorption of As(V). This result suggested a significant decrease in the host anions in the interlayer region of Mn/Mg/Fe-LDH that resulted from the anion exchange phenomenon. However, the FTIR data cannot distinguish between NO_3^- and CO_3^{2-} anions (Goh et al., 2009).

The XPS data (Figure S6) indicated that NO_3^- anions in its interlayer region played a more important role in exchanging As(V) anions than CO_3^{2-} anions. This is because a remarkable decease in (1) the atomic percentage of N element (Table S1) from 2.54% to 0.14% after adsorption of As(V) and (2) the intensity of the important peak at approximately 407 eV (Figure S6). Goh et al. (2009) also reported a remarkable decrease in N% from 2.9% to nearly 0% (XPS data) after adsorbing As(V) by NO_3-intercalated Mg/Al-LDH. Equation 17 gives an anion exchange stoichiometry between As(V) anions in solution and the host NO_3^- anions in the interlayer region of Mn/Mg/Fe-LDH without considering exchange between As(V) and CO_3^{2-} anions (Goh et al., 2009).

$$HAsO_4^{2-}(aq) + 2NO_3^- - LDH(s) \rightleftharpoons 2NO_3^-(aq) + HAsO_4^{2-} - LDH(s) \quad (17)$$

Furthermore, the XRD data (Figure 1) confirmed that the import role of anion exchange between As(V) anions and NO_3^- anions because of the disappearance of the relevant peak at 29.4° ($NaNO_3$) for As(V)-laden Mn/Mg/Fe-LDH. In contrast, Figure S5 and Table S1 show that after adsorption of As(V), the presence of the host CO_3^{2-} anions in the interlayer region of Mn/Mg/Fe-LDH still maintained.

As discussed at Section 3.10.1, the anion exchange does not make Mn/Mg/Fe-LDH in loss of its original structure. However, Figure 1 shows that Mn/Mg/Fe-LDH lost its original structure after adsorption of As(V). The result suggested that anion exchange might occur in the first period of the adsorption process. This hypothesis can be supported by the desorption study (Section 3.8). After the exchange process, the guest As(V) anions in the interlayer region

of Mn/Mg/Fe-LDH contacted to Fe^{2+}. The reduction of As(V) to As(III) was described in Equations 13–14. The redox reactions that occurred in the interlayer region might lead to destroy the original layer structure of Mn/Mg/Fe-LDH (Figure 1). This conclusion might be support by changing the textural properties (i.e., S_{BET}) of Mn/Mg/Fe-LDH after adsorbing As(V) anions (Figure 2).

3.10.5. Pore-filling mechanism

In essence, pore filling often plays a more important role in the adsorption mechanism of organic pollutants than inorganic pollutants. Many authors ignored the role of pore-filling mechanism when they interpreted the adsorption process of arsenic (Liu et al., 2006; Huang et al., 2015; Guo et al., 2017; Ding et al., 2018; Lu et al., 2018; Mubarak et al., 2018; Choong et al., 2021). If pore-filling mechanism is dominant, the S_{BET} value of LDH should decease after adsorption. For example, Wang et al. (2021) found that the S_{BET} value of Fe/Mn-C-LDH decreased from 170.5 to 68.2 m^2/g after absorbing As(III) or to 92.1 m^2/g after absorbing As(V). However, Figure 2 shows that the S_{BET} value of Mn/Mg/Fe-LDH remarkably increased from 75.2 to 156 m^2/g after the adsorption process. The result might because Mn/Mg/Fe-LDH lost its original layer structure caused by the redox reactions (Section 3.10.4).

3.10.6. Isomorphic substitution

Isomorphic substitution is commonly found for the adsorption of cation metals (Cr^{3+}, Pb^{2+}, Cd^{2+}, etc.) by clay minerals like LDH. For example, Cr^{3+} ions in solution can isomorphically substitute to Al^{3+} in the LDH structure (i.e., Mg/Al-LDH) after the adsorption process. This is because of a similar radius between them (Cr^{3+} and Al^{3+} of 0.052 nm and 0.054 nm, respectively) (Chao et al., 2018; Tran et al., 2019). Although As(V) anions was reduced to As(III) ions when they contact with Mn/Mg/Fe-LDH, As(III) exists as a charge-neutral species. Therefore, adsorption mechanism involved in isomorphic substitution was ruled out in this study. This mechanism was not reported for adsorbing arsenic onto other LDH

materials (Liu et al., 2006; Goh et al., 2009; Bagherifam et al., 2014; Huang et al., 2015; Guo et al., 2017; Hudcová et al., 2017; Lu et al., 2018; Mubarak et al., 2018; Liu et al., 2019; Choong et al., 2021; Wang et al., 2021).

3.10.7. Hydrogen bonding interaction

Some authors reported that the adsorption of As(III) and As(V) by LDH-based materials through hydrogen bonding (Hudcová et al., 2017; Liu et al., 2019; Choong et al., 2021). For example, Choong et al. (2021) concluded that hydrogen bonding is one of the most important adsorption mechanisms of As(III) and As(V) onto the polymers-embedded Mg/Fe-LDH. However, the authors did not give any convincing evidence for the existence of such interaction (Choong et al., 2021). In fact, it is very hard to interpret the presence of H-bonding interactions between Mn/Mg/Fe-LDH and As by FTIR, XPS, or even EXAFS (Wang and Mulligan, 2008; Wang et al., 2009).

In contrast, many researchers ignored this interaction when they discussed the adsorption mechanisms of arsenic by the LDH-based materials (Liu et al., 2006; Goh et al., 2009; Wang et al., 2009; Bagherifam et al., 2014; Huang et al., 2015; Guo et al., 2017; Lu et al., 2018; Mubarak et al., 2018; Wang et al., 2021) and other materials such as zero-valent iron (Bang et al., 2005), birnessite (Tournassat et al., 2002), gibbsite (Liu et al., 2006), and aluminum-enriched biochar (Ding et al., 2018). This mechanism might also exit in the adsorption systems. However, its contribution might be negligible.

3.11. Possible adsorption mechanism of adsorption mechanism of As(III) ions

Some authors reported that As(III) was reduced to As(0) after adsorption (Bang et al., 2005). However, this reduction was ruled out in this study. Figure 9 shows that As(0) species did not exist in the As(III)-laden Mn/Mg/Fe-LDH.

Arsenite exits as a predominantly uncharged species ($H_3AsO_3°$; Figure S1) in aqueous solution at pH 7.0. Therefore, the out-sphere surface complex was ruled out. However, the

721 adsorption phenomenon of As(III) by Mn/Mg/Fe-LDH was very similar to that of As(V),
722 especially the adsorption studies of effects of pH and foreign anions. Therefore, it is highly
723 expected that As(III) ions were oxidized to As(V) anions during the adsorption process of
724 As(III). The oxidation phenomenon of As(III) to As(V) by LDH-based materials have been
725 reported by many scholars, such as Cl-intercalated Mg/Fe (Guo et al., 2017) and granular
726 Mg/Fe-LDH (Choong et al., 2021). The oxidation process by Mn(VI) can occur two steps
727 (Equations 18–19). The redox reaction can be overall expressed as Equation 20 (Tournassat et
728 al., 2002).

$$H_3AsO_3^0 + 2MnO_2 + H_2O \rightleftharpoons H_2AsO_4^- + 2MnOOH + H^+ \quad (18)$$

$$H_3AsO_3^0 + 2MnOOH + 3H^+ \rightleftharpoons H_2AsO_4^- + 2Mn^{2+} + 3H_2O \quad (19)$$

$$H_3AsO_3^0 + MnO_2 + H^+ \rightleftharpoons H_2AsO_4^- + Mn^{2+} + H_2O \quad (20)$$

729 However, the oxidation process might occur at the first period of the adsorption process
730 (i.e., 10 min contact). The XPS data showed BE [As 3d] = 49.59 eV and 44.89 eV (Figure 9a)
731 and BE [As 2p3] = 1327.8 eV (Table S1). Those values are close the BE values of As(V) that
732 have been reported elsewhere (Choong et al., 2021; Wang et al., 2021). For example, Choong
733 et al. (2021) reported that the As species in the polymers-embedded Mg/Fe-LDH after
734 adsorption were As(V) [BE at 1326.1 eV (As 2p3) and 44.72 eV (As 3d3)] and As(III) [1325.6
735 eV (As 2p3) and 43.97 eV (As 3d3)].

736 In addition, Figure 9b shows that after the 10-min adsorption of As(III), the As(V) species
737 (61.20%) predominated in Mn/Mg/Fe-LDH compared to As(III) one (38.80%). However, after
738 the 48-h adsorption of As(III), the percentages of As(V) only accounted for 39.77% (Figure
739 9c). The result suggested the existence of the first redox reaction (Equation 19); as a result,
740 As(III) was oxidized to As(V). The adsorption mechanisms of the oxidized As(V) anions by
741 Mn/Mg/Fe-LDH might occur as the case of adsorbing As(VI) (Section 3.10). The XPS data
742 (Figure 9c) confirmed that there was the existence of the second redox reaction (Equations 13–

14); as a result, the oxidized As(V) was then reduced to As(III). The original and reduced As(III) ions were adsorbed by Mn/Mg/Fe-LDH through the dominant inner-sphere complexation. As(III) is often more favourable than As(V) in complexing with the OH groups in adsorbents. Some authors (Hong et al., 2014; Penke et al., 2021) found that As(III) was more easily to adsorbed by LDH through the strong in-sphere surface complexation. This conclusion was supported by the O 1s spectrum in Figure 4a (or Figure S7) through a remarkable decrease in the density of the peaks at ~529 eV (M–O or M–O–M) and ~533 eV ($M–OH_2^+$).

Figure S6 (or Table S1) shows that two involved processes—the oxidation of As(III) to As(V) anions as well as anion exchange between the oxidized As(V) anions and the host anions (NO_3^-) in the interlayer region of Mn/Mg/Fe-LDH—occurred very fast (~10 min). After 10-min contact, the species of As(V) in the laden Mn/Mg/Fe-LDH were dominant (61.20%; Figure 9b) than those of As(III).

The oxidation and reduction occurred simultaneously in the adsorption system along with the other phenomena (adsorption and desorption). As a result, Mn/Mg/Fe-LDH lost its original structure after the completed adsorption process of As(III) (Figure 1).

3.13. Application of Mn/Mg/Fe-LDH for eliminating arsenic from groundwater

Mn/Mg/Fe-LDH was applied for removing As from real groundwater. The groundwater samples from the wells of ten households were collected in the Phuong Tu commune, Ung Hoa district, Hanoi, Vietnam. The basic characteristics of the groundwater are presented in Table S7. The batch adsorption experiment was contacted under the following conditions: 1.0 g/L, room temperature (~31 °C), pH (not adjusted; pH = 6.81–7.32), and 24 h.

The concentrations of the raw groundwaters from ten local wells (before sand filtration) ranged from 45 ppb to 92 ppb (Table S8). After the adsorption process, the residual As concentrations (0.35–7.9 ppb) were detected below the Vietnam and WHO drinking water standards (10 ppb) (Regis et al., 2022). Similarly, Lu et al. (2018) used the calcinated Ca/Fe-

LDH (1.0 g/L) for the decontamination of arsenic (mainly arsenate form) from the water samples of the river. They found that the concentrations of As after adsorption was 1.7 ppb (C_o = 30 ppb and pH = 7.12) and 9.2 ppb (C_o = 1,110 ppb and pH = 7.62). Table S8 shows that the removal efficiency of As from the groundwaters ranged from 91.41% to 99.22%. Therefore, Mn/Mg/Fe-LDH can serve as a promising material for the real applications.

4. Conclusions

The Mn/Mg/Fe-LDH material (acting as catalyst and adsorbent) was successfully synthesized from three salts of metals [i.e., $Mg(NO_3)_2$, $Mn(NO_3)_2$, and $Fe(NO_3)_3$] through a simple co-precipitation process. The basal spacing of Mn/Mg/Fe-LDH was 0.757 nm. The host anions (NO_3^- and CO_3^2) in its internal region were identified by the XRD FTIR, and XPS techniques. Mn/Mg/Fe-LDH possessed a positively charged surface when pH solution was lower than its pH_{IEP} of 10.15. The Mn/Mg/Fe-LDH adsorbent was mesoporous material (average pore with of 14.2 nm), with its S_{BET} and V_{Total} being 75.2 m^2/g and 0.267 cm^3/g.

The process of As(III) adsorption onto Mn/Mg/Fe-LDH was relatively similar to that of As(V). The adsorption capacity of Mn/Mg/Fe-LDH was significantly affected by the presence of foreign anions in solution. The adsorption trend followed the order of no competition (absence of foreign anions) > the presence of Cl^- anion > SO_4^{2-} anion > HPO_4^{2-} anion > CO_3^{2-} anion > SiO_3^{2-} anion > five foreign anions (Cl^-, SO_4^{2-}, CO_3^{2-}, SiO_3^{2-}, and HPO_4^{2-}). Mn/Mg/Fe-LDH exhibited a higher capacity of toxic As(III) adsorption than As(V), with the Langmuir maximum adsorption capacity at 25 °C and pH 7.0. It was 56.1 mg/g for As(III) and 32.2 mg/g for As(V). In this pH scenario, the amounts of Mn, Mg and Fe leached after the adsorption process were smaller than the Vietnamese government's standard limit according to the QCVN 01:2009/BYT: Vietnam national technical regulation on drinking water quality. Desorption study demonstrated that adsorption is highly irreversible. This meant that the release of As from laden Mn/Mg/Fe-LDH into the environment was negligible. Mn/Mg/Fe-LDH can remove

efficiently As from groundwater, with the initial As concentrations decreasing from 45–92 ppb to 0.35–7.9 ppb. XPS data confirmed that the removal mechanisms were oxidation-coupled adsorption for As(III) and reduction-coupled adsorption for As(V).

Mn/Mg/Fe-LDH can serve as a promising catalyst and adsorbent for removing highly toxic As(III) ions and As(III) anions from water.

Acknowledgement

This study was financially supported by the Aus4Innovation program—a development cooperation initiative funded by the Australian Department of Foreign Affairs and Trade and InnovationXchange, and managed by the Commonwealth Scientific and Industrial Research Organization, in partnership with the Ministry of Science and Technology of Vietnam. The first author thanks University of Technology Sydney for a PhD studentship.

REFERENCES

Asiabi, H., Yamini, Y., Shamsayei, M., 2017. Highly selective and efficient removal of arsenic (V), chromium (VI) and selenium (VI) oxyanions by layered double hydroxide intercalated with zwitterionic glycine. J. Hazard. Mater. 339, 239-247.

Asiabi, H., Yamini, Y., Shamsayei, M., 2017. Highly selective and efficient removal of arsenic(V), chromium(VI) and selenium(VI) oxyanions by layered double hydroxide intercalated with zwitterionic glycine. J. Hazard. Mater. 339, 239-247.

Bagherifam, S., Komarneni, S., Lakzian, A., Fotovat, A., Khorasani, R., Huang, W., Ma, J., Wang, Y., 2014. Evaluation of Zn–Al–SO4 layered double hydroxide for the removal of arsenite and arsenate from a simulated soil solution: Isotherms and kinetics. Appl. Clay Sci. 95, 119-125.

Bai, Y., Yang, T., Liang, J., Qu, J., 2016. The role of biogenic Fe-Mn oxides formed in situ for arsenic oxidation and adsorption in aquatic ecosystems. Water Res. 98, 119-127.

Bang, S., Johnson, M.D., Korfiatis, G.P., Meng, X., 2005. Chemical reactions between arsenic and zero-valent iron in water. Water Res. 39, 763-770.

819 Berg, M., Tran, H.C., Nguyen, T.C., Pham, H.V., Schertenleib, R., Giger, W., 2001. Arsenic
820 contamination of groundwater and drinking water in Vietnam: a human health
821 threat. Environ. Sci. Technol. 35, 2621-2626.

822 Córdova Reyes, I., Salmones, J., Zeifert, B., Contreras, J.L., Rojas, F., 2014. Transesterification
823 of canola oil catalized by calcined Mg–Al hydrotalcite doped with nitratine. Chem.
824 Eng. Sci. 119, 174-181.

825 Chao, H.-P., Wang, Y.-C., Tran, H.N., 2018. Removal of hexavalent chromium from
826 groundwater by Mg/Al-layered double hydroxides using characteristics of in-situ
827 synthesis. Environ. Pollut. 243, 620-629.

828 Choong, C.E., Wong, K.T., Jang, S.B., Saravanan, P., Park, C., Kim, S.-H., Jeon, B.-H., Choi,
829 J., Yoon, Y., Jang, M., 2021. Granular Mg-Fe layered double hydroxide prepared
830 using dual polymers: Insights into synergistic removal of As(III) and As(V). J.
831 Hazard. Mater. 403, 123883.

832 Chubar, N., Gerda, V., Megantari, O., Mičušík, M., Omastova, M., Heister, K., Man, P.,
833 Fraissard, J., 2013. Applications versus properties of Mg–Al layered double
834 hydroxides provided by their syntheses methods: Alkoxide and alkoxide-free sol–
835 gel syntheses and hydrothermal precipitation. Chem. Eng. J. 234, 284-299.

836 Ding, Z., Xu, X., Phan, T., Hu, X., Nie, G., 2018. High adsorption performance for As(III) and
837 As(V) onto novel aluminum-enriched biochar derived from abandoned Tetra Paks.
838 Chemosphere 208, 800-807.

839 Frau, F., Addari, D., Atzei, D., Biddau, R., Cidu, R., Rossi, A., 2010. Influence of major anions
840 on As (V) adsorption by synthetic 2-line ferrihydrite. Kinetic investigation and XPS
841 study of the competitive effect of bicarbonate. Water Air Soil Pollut. 205, 25-41.

842 Goh, K.-H., Lim, T.-T., Dong, Z., 2008. Application of layered double hydroxides for removal
843 of oxyanions: A review. Water Res. 42, 1343-1368.

844 Goh, K.-H., Lim, T.-T., Dong, Z., 2009. Enhanced arsenic removal by hydrothermally treated
845 nanocrystalline Mg/Al layered double hydroxide with nitrate intercalation. Environ.
846 Sci. Technol. 43, 2537-2543.

847 Guo, Q., Cao, Y., Yin, Z., Yu, Z., Zhao, Q., Shu, Z., 2017. Enhanced removal of arsenic from
848 water by synthetic nanocrystalline iowaite. Sci. Rep. 7, 17546.

849 Guo, X.L., Liu, X.Y., Hao, X.D., Zhu, S.J., Dong, F., Wen, Z.Q., Zhang, Y.X., 2016. Nickel-
850 manganese layered double hydroxide nanosheets supported on nickel foam for

high-performance supercapacitor electrode materials. Electrochim. Acta 194, 179-186.

Haynes, W.M., 2010. Electrochemical series. CRC handbook of chemistry and physics. CRC press.

Hong, J., Zhu, Z., Lu, H., Qiu, Y., 2014. Synthesis and arsenic adsorption performances of ferric-based layered double hydroxide with α-alanine intercalation. Chem. Eng. J. 252, 267-274.

Huang, P.-P., Cao, C.-Y., Wei, F., Sun, Y.-B., Song, W.-G., 2015. MgAl layered double hydroxides with chloride and carbonate ions as interlayer anions for removal of arsenic and fluoride ions in water. RSC Adv. 5, 10412-10417.

Hudcová, B., Veselská, V., Filip, J., Číhalová, S., Komárek, M., 2017. Sorption mechanisms of arsenate on Mg-Fe layered double hydroxides: A combination of adsorption modeling and solid state analysis. Chemosphere 168, 539-548.

Iruretagoyena Ferrer, D., 2016. Influence of alkali metals on layered double hydroxides supported on graphene oxide for CO_2 adsorption. in: Iruretagoyena Ferrer, D. (Ed.). Supported Layered Double Hydroxides as CO_2 Adsorbents for Sorption-enhanced H_2 Production. Springer International Publishing, Cham, pp. 115-139.

Jiao, Y.-N., Hou, W.-G., 2007. Effects of structural charges on points of zero charge and intrinsic surface reaction equilibrium constants of Zn–Al and Zn–Al–Fe hydrotalcite-like compounds. Colloids Surf. A 296, 62-66.

Johnston, R.B., Singer, P.C., 2007. Solubility of symplesite (ferrous arsenate): implications for reduced groundwaters and other geochemical environments. Soil Sci. Soc. Am. J. 71, 101-107.

Karmacharya, M.S., Gupta, V.K., Tyagi, I., Agarwal, S., Jha, V.K., 2016. Removal of As(III) and As(V) using rubber tire derived activated carbon modified with alumina composite. J. Mol. Liq. 216, 836-844.

Kim, K.-W., Chanpiwat, P., Hanh, H.T., Phan, K., Sthiannopkao, S., 2011. Arsenic geochemistry of groundwater in Southeast Asia. Front. Med. 5, 420-433.

Kong, S., Wang, Y., Hu, Q., Olusegun, A.K., 2014. Magnetic nanoscale Fe–Mn binary oxides loaded zeolite for arsenic removal from synthetic groundwater. Colloids Surf. A 457, 220-227.

Lee, S.-H., Tanaka, M., Takahashi, Y., Kim, K.-W., 2018. Enhanced adsorption of arsenate and antimonate by calcined Mg/Al layered double hydroxide: Investigation of comparative adsorption mechanism by surface characterization. Chemosphere 211, 903-911.

Lenoble, V., Laclautre, C., Deluchat, V., Serpaud, B., Bollinger, J.-C., 2005. Arsenic removal by adsorption on iron(III) phosphate. J. Hazard. Mater. 123, 262-268.

Li, Y., Gao, B., Wu, T., Sun, D., Li, X., Wang, B., Lu, F., 2009. Hexavalent chromium removal from aqueous solution by adsorption on aluminum magnesium mixed hydroxide. Water Res. 43, 3067-3075.

Lièvremont, D., Bertin, P.N., Lett, M.-C., 2009. Arsenic in contaminated waters: Biogeochemical cycle, microbial metabolism and biotreatment processes. Biochimie 91, 1229-1237.

Lin, L., Qiu, W., Wang, D., Huang, Q., Song, Z., Chau, H.W., 2017. Arsenic removal in aqueous solution by a novel Fe-Mn modified biochar composite: Characterization and mechanism. Ecotoxicol. Environ. Saf. 144, 514-521.

Liu, J., Wu, P., Li, S., Chen, M., Cai, W., Zou, D., Zhu, N., Dang, Z., 2019. Synergistic deep removal of As(III) and Cd(II) by a calcined multifunctional MgZnFe-CO3 layered double hydroxide: Photooxidation, precipitation and adsorption. Chemosphere 225, 115-125.

Liu, Y.T., Wang, M.K., Chen, T.Y., Chiang, P.N., Huang, P.M., Lee, J.F., 2006. Arsenate sorption on lithium/aluminum layered double hydroxide intercalated by chloride and on gibbsite: sorption isotherms, envelopes, and spectroscopic studies. Environ. Sci. Technol. 40, 7784-7789.

Liu, Y.T., Wang, M.K., Chen, T.Y., Chiang, P.N., Huang, P.M., Lee, J.F., 2006. Arsenate Sorption on Lithium/Aluminum Layered Double Hydroxide Intercalated by Chloride and on Gibbsite: Sorption Isotherms, Envelopes, and Spectroscopic Studies. Environ. Sci. Technol. 40, 7784-7789.

Lu, H., Liu, S., Zhang, H., Qiu, Y., Zhao, J., Zhu, Z., 2018. Decontamination of arsenic in actual water samples by calcium containing layered double hydroxides from a convenient synthesis method. Water 10, 1150.

Lyklema, J., 1995. Fundamentals of interface and colloid science. Vol. II: Solid-Liquid Interfaces. 1995. San Diego: Academic Press.

914 Mohammadi, N., Pourreza, K., Bahrami Adeh, N., Omidvar, M., 2021. Defective mesoporous
915 carbon/MnO2 nanocomposite as an advanced electrode material for supercapacitor
916 application. J. Alloys Compd. 883, 160874.

917 Mubarak, M., Jeon, H., Islam, M.S., Yoon, C., Bae, J.-S., Hwang, S.-J., Choi, W.S., Lee, H.-J.,
918 2018. One-pot synthesis of layered double hydroxide hollow nanospheres with
919 ultrafast removal efficiency for heavy metal ions and organic contaminants.
920 Chemosphere 201, 676-686.

921 Neppolian, B., Celik, E., Choi, H., 2008. Photochemical oxidation of arsenic(III) to arsenic(V)
922 using peroxydisulfate ions as an oxidizing agent. Environ. Sci. Technol. 42, 6179-
923 6184.

924 Nguyen, T.H., Tran, H.N., Vu, H.A., Trinh, M.V., Nguyen, T.V., Loganathan, P., Vigneswaran,
925 S., Nguyen, T.M., Trinh, V.T., Vu, D.L., Nguyen, T.H.H., 2020. Laterite as a low-
926 cost adsorbent in a sustainable decentralized filtration system to remove arsenic
927 from groundwater in Vietnam. Sci. Total Environ. 699, 134267.

928 Nguyen, T.H., Tran, H.N., Vu, H.A., Trinh, M.V., Nguyen, T.V., Loganathan, P., Vigneswaran,
929 S., Nguyen, T.M., Vu, D.L., Nguyen, T.H.H., 2020. Laterite as a low-cost adsorbent
930 in a sustainable decentralized filtration system to remove arsenic from groundwater
931 in Vietnam. Sci. Total Environ. 699, 134267.

932 Otgonjargal, E., Kim, Y.-S., Park, S.-M., Baek, K., Yang, J.-S., 2012. Mn–Fe layered double
933 hydroxides for adsorption of As(III) and As(V). Sep. Sci. Technol. 47, 2192-2198.

934 Pavlovic, M., Huber, R., Adok-Sipiczki, M., Nardin, C., Szilagyi, I., 2016. Ion specific effects
935 on the stability of layered double hydroxide colloids. Soft Matter 12, 4024-4033.

936 Penke, Y.K., Yadav, A.K., Malik, I., Tyagi, A., Ramkumar, J., Kar, K.K., 2021. Insights of
937 arsenic (III/V) adsorption and electrosorption mechanism onto multi synergistic
938 (redox-photoelectrochemical-ROS) aluminum substituted copper ferrite
939 impregnated rGO. Chemosphere 267, 129246.

940 Regis, A.O., Vanneste, J., Acker, S., Martínez, G., Ticona, J., García, V., Alejo, F.D., Zea, J.,
941 Krahenbuhl, R., Vanzin, G., Sharp, J.O., 2022. Pressure-driven membrane
942 processes for boron and arsenic removal: pH and synergistic effects. Desalination
943 522, 115441.

944 Rosanoff, A., 2013. The high heart health value of drinking-water magnesium. Med.
945 Hypotheses 81, 1063-1065.

Smedley, P.L., Kinniburgh, D.G., 2002. A review of the source, behaviour and distribution of arsenic in natural waters. Appl. Geochem. 17, 517-568.

Soma, M., Tanaka, A., Seyama, H., Satake, K., 1994. Characterization of arsenic in lake sediments by X-ray photoelectron spectroscopy. Geochim. Cosmochim. Acta 58, 2743-2745.

Tian, Z., Feng, Y., Guan, Y., Shao, B., Zhang, Y., Wu, D., 2017. Opposite effects of dissolved oxygen on the removal of As(III) and As(V) by carbonate structural Fe(II). Sci. Rep. 7, 17015.

Tournassat, C., Charlet, L., Bosbach, D., Manceau, A., 2002. Arsenic(III) oxidation by birnessite and precipitation of manganese(II) arsenate. Environ. Sci. Technol. 36, 493-500.

Tran, H.N., Nguyen, D.T., Le, G.T., Tomul, F., Lima, E.C., Woo, S.H., Sarmah, A.K., Nguyen, H.Q., Nguyen, P.T., Nguyen, D.D., Nguyen, T.V., Vigneswaran, S., Vo, D.-V.N., Chao, H.-P., 2019. Adsorption mechanism of hexavalent chromium onto layered double hydroxides-based adsorbents: A systematic in-depth review. J. Hazard. Mater. 373, 258-270.

Triviño, M.L.T., Hiremath, V., Seo, J.G., 2018. Stabilization of NaNO3-promoted magnesium oxide for high-temperature CO2 capture. Environ. Sci. Technol. 52, 11952-11959.

Varga, G., Somosi, Z., Kónya, Z., Kukovecz, Á., Pálinkó, I., Szilagyi, I., 2021. A colloid chemistry route for the preparation of hierarchically ordered mesoporous layered double hydroxides using surfactants as sacrificial templates. J. Colloid Interface Sci. 581, 928-938.

Vucelic, M., Jones, W., Moggridge, G.D., 1997. Cation ordering in synthetic layered double hydroxides. Clays Clay Miner. 45, 803-813.

Wang, J., Zhang, T., Li, M., Yang, Y., Lu, P., Ning, P., Wang, Q., 2018. Arsenic removal from water/wastewater using layered double hydroxide derived adsorbents, a critical review. RSC Adv. 8, 22694-22709.

Wang, K., Liu, Y., Ding, Z., Chen, Z., Xu, X., Wang, M., Lu, T., Pan, L., 2021. Chloride pre-intercalated CoFe-layered double hydroxide as chloride ion capturing electrode for capacitive deionization. Chem. Eng. J., 133578.

976 Wang, S.-L., Liu, C.H., Wang, M.K., Chuang, Y.H., Chiang, P.N., 2009. Arsenate adsorption
977 by Mg/Al–NO3 layered double hydroxides with varying the Mg/Al ratio. Appl.
978 Clay Sci. 43, 79-85.

979 Wang, S., Mulligan, C.N., 2008. Speciation and surface structure of inorganic arsenic in solid
980 phases: A review. Environ. Int. 34, 867-879.

981 Wang, Y., Gao, Y., Zhu, Z., Zhang, L., Zhao, N., Fang, Y., Zhu, Y., Liu, G., 2021. Enhanced
982 arsenic removal from aqueous solution by Fe/Mn-C layered double hydroxide
983 composite. Adsorp. Sci. Technol. 2021, 8891643.

984 Yang, L., Shahrivari, Z., Liu, P.K.T., Sahimi, M., Tsotsis, T.T., 2005. Removal of trace levels
985 of arsenic and selenium from aqueous solutions by calcined and uncalcined layered
986 double hydroxides (LDH). Ind. Eng. Chem. Res. 44, 6804-6815.

987 Yu, X.-Y., Luo, T., Jia, Y., Xu, R.-X., Gao, C., Zhang, Y.-X., Liu, J.-H., Huang, X.-J., 2012.
988 Three-dimensional hierarchical flower-like Mg–Al-layered double hydroxides:
989 highly efficient adsorbents for As(V) and Cr(VI) removal. Nanoscale 4, 3466-3474.

990 Zhang, Y., Cao, J., Li, J., Yuan, Z., Li, D., Wang, L., Han, W., 2022. Self-assembled Cobalt-
991 doped NiMn-layered double hydroxide (LDH)/V2CTx MXene hybrids for
992 advanced aqueous electrochemical energy storage properties. Chem. Eng. J. 430,
993 132992.

994 Zhou, W., Kong, Z., Wu, Z., Yang, S., Wang, Y., Liu, Y., 2021. Efficient oxidation of biomass
995 derived 5-hydroxymethylfurfural into 2,5-diformylfuran catalyzed by NiMn
996 layered double hydroxide. Catal. Commun. 151, 106279.

997

Table 1. The effect of solution pH on the structural stability of LDH and the release of metal ions (mg/L) from LDH after an equilibrium adsorption

pH	Distilled water			As(V) solution			As(III) solution		
	Fe	Mn	Mg	Fe	Mn	Mg	Fe	Mn	Mg
2	11.25	150	50.0	0.045	35.8	30.1	0.071	58.5	40.1
3	<0.01	<0.01	11.7	0.045	0.63	8.14	0.048	0.76	8.72
4	<0.01	<0.01	4.96	0.039	0.26	4.22	0.060	0.25	4.36
5	<0.01	<0.01	4.30	0.093	0.33	3.34	0.050	0.31	4.07
6	<0.01	<0.01	3.59	0.050	0.22	3.05	0.057	0.26	3.98
7	<0.01	<0.01	3.91	0.044	0.22	1.79	0.065	0.25	3.40
8	<0.01	<0.01	3.54	0.077	0.14	1.63	0.059	0.15	3.26
9	<0.01	<0.01	3.47	0.065	0.17	1.16	0.056	0.15	2.67
10	<0.01	<0.01	2.63	0.101	0.11	—	0.063	0.051	1.95

Note: The concentrations of metal ions (mg/L) were released from distilled water were denoted as the blank sample (without arsenic adsorption). The limitation (established by the Vietnam national technical regulation on drinking water quality; QCVN 01:2009/BYT) for both total Fe (Fe^{2+} and Fe^{3+}) and Mn in drinking water was 0.3 mg/L. The above values were averaged from the duplicates, and their SD values were less than 10%.

Table 2. Isotherm adsorption parameters for As(V) and As(III) uptake onto Mg/Mn/Fe-LDH

	Unit	As(V)			As(III)		
		7 °C	25 °C	50 °C	7 °C	25 °C	50 °C
1. Langmuir model							
Q_{max}	mg/g	21.9±	32.2	24.0	37.8	56.1	39.6
K_L	L/mg	0.063	0.138	0.096	76.3	126	95.7
adj-R^2	—	0.981	0.954	0.990	0.996	0.988	0.984
red-χ^2	—	0.964	6.096	0.790	0.682	5.230	3.066
2. Freundlich model							
K_F	$(mg/g)/(mg/L)^n$	5.61	9.89	5.96	9.32	13.3	10.8
n_F	—	0.255	0.232	0.272	0.275	0.283	0.261
R^2	—	0.987	0.977	0.949	0.959	0.927	0.974
χ^2	—	0.662	3.096	3.838	6.591	32.065	4.891
3. Redlich–Peterson model							
K_{RP}	L/g	3.20	16.3	2.90	2.88	8.32	6.20
a_{RP}	$(mg/L)^{-g}$	0.345	1.192	0.172	0.076	0.195	0.279
g	—	0.838	0.832	0.930	1.000	0.945	0.883
R^2	—	0.991	0.986	0.992	0.995	0.989	0.988
χ^2	—	0.460	1.792	0.607	0.854	4.695	2.239
4. Langmuir-Freundlich model							
Q_{LF}	mg/g	29.1	45.4	25.0	38.1	58.0	46.4
K_{LF}	L/mg	0.027	0.038	0.086	0.075	0.112	0.062
n_{LF}	—	0.568	0.474	0.882	0.977	0.895	0.686
R^2	—	0.993	0.993	0.989	0.995	0.988	0.991
χ^2	—	0.356	0.989	0.827	0.845	5.395	1.630
5. Khan model							
Q_K	mg/g	10.7	13.4	17.8	39.4	44.3	24.4
K_K	L/mg	0.248	0.897	0.156	0.072	0.181	0.227
n_K	—	0.819	0.826	0.911	1.016	0.931	0.865
R^2	—	0.990	0.985	0.993	0.995	0.990	0.987
χ^2	—	0.485	1.937	0.560	0.844	4.589	2.400

Note: Average Q_{max} ± SE values: 37.8±0.80, 56.1±1.47, and 39.6±1.58.

Table 3. Thermodynamic parameters ($\Delta H°$ and $\Delta S°$) of the As(III) and As(V) adsorption by Mg/Mn/Fe-LDH at two operation temperatures

Temperature	As(III)		As(V)	
	$\Delta H°$	$\Delta S°$	$\Delta H°$	$\Delta S°$
1. Based on K_L of the Langmuir model				
288–298K	19.3	141	29.9	172
298–323K	–8.75	46.7	–11.44	32.3
2. Based on K_{LF} the Langmuir–Freundlich model				
288–298K	13.1	110	15.41	121
298–323K	25.7	152	–18.64	6.75
3. Based on K_K the Khan model				
288–298K	49.5	258	35.81	194
298–323K	–55.9	–95.2	7.17	97.4

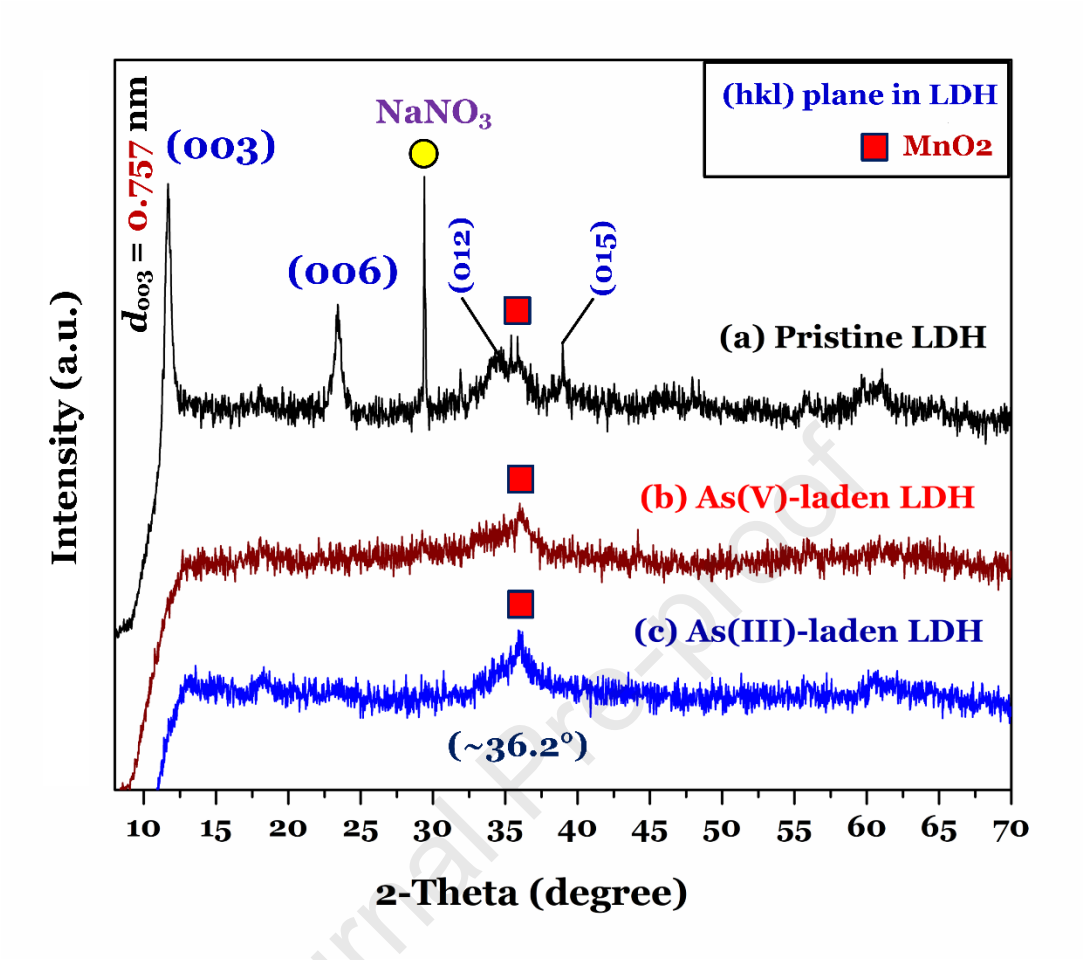

Figure 1. XRD pattern of Mn/Mg/Fe-LDH before and after adsorption of As(III) ions and As(V) anions (Adsorption conditions: 1.0 g/L, C_o = 50 mg/L, 24 h, pH = 7.0, and 25 °C)

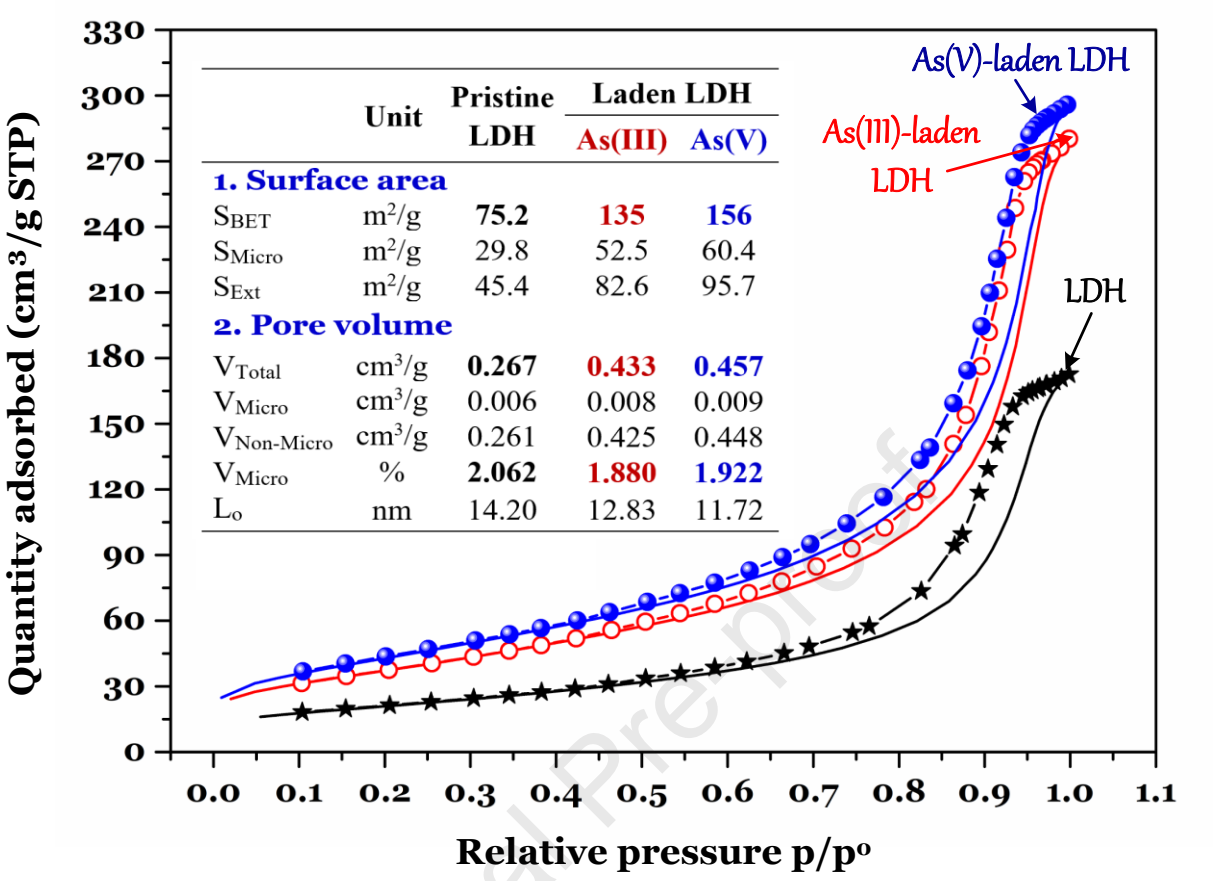

Figure 2. Nitrogen adsorption/desorption isotherm at 77 K of pristine and laden Mn/Mg/Fe-LDH adsorbents (Adsorption conditions: 1.0 g/L, C_o = 50 mg/L, 24 h, pH = 7.0, and 25 °C)

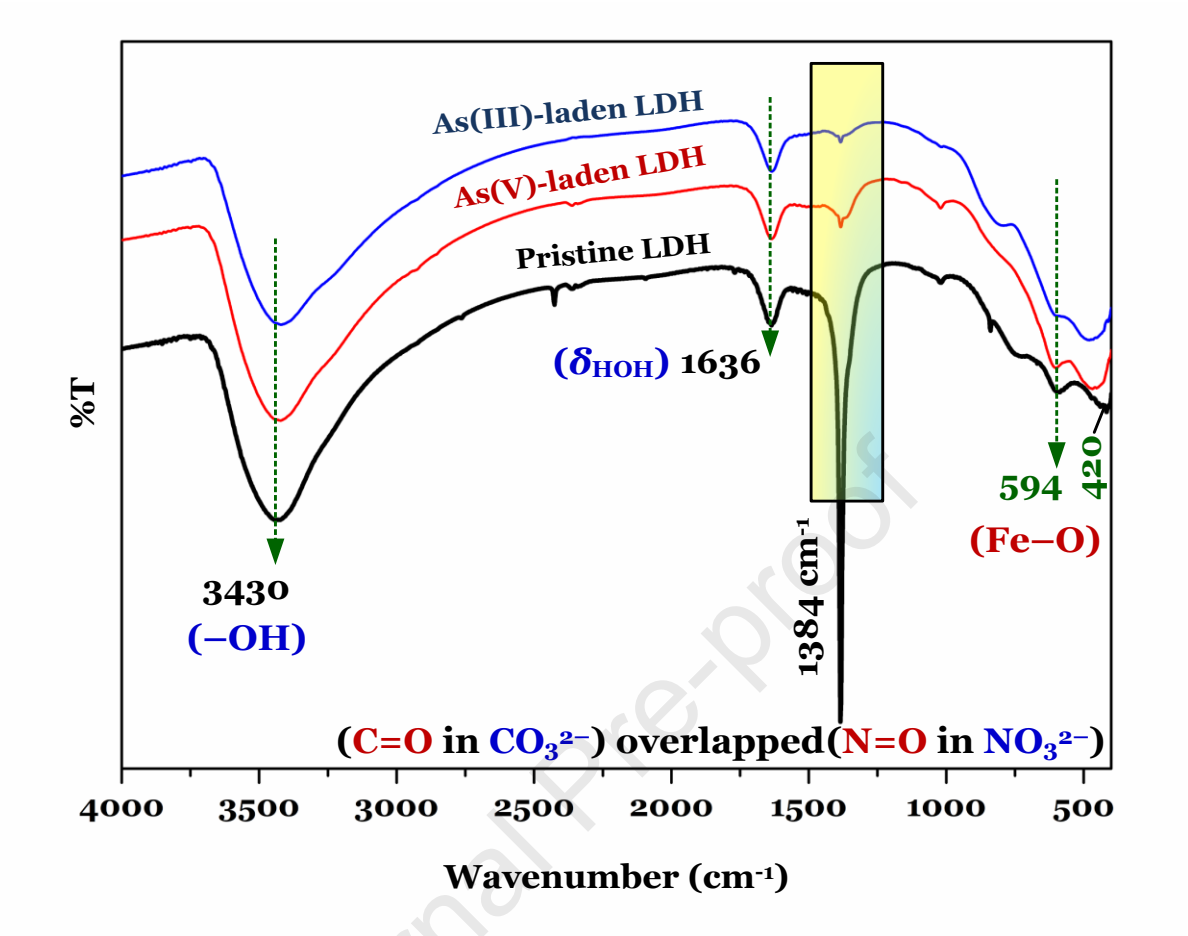

Figure 3. FTIR spectrum of Mn/Mg/Fe-LDH before and after adsorption of arsenic ions (Adsorption conditions: 1.0 g/L, C_o = 50 mg/L, 24 h, pH = 7.0, and 25 °C)

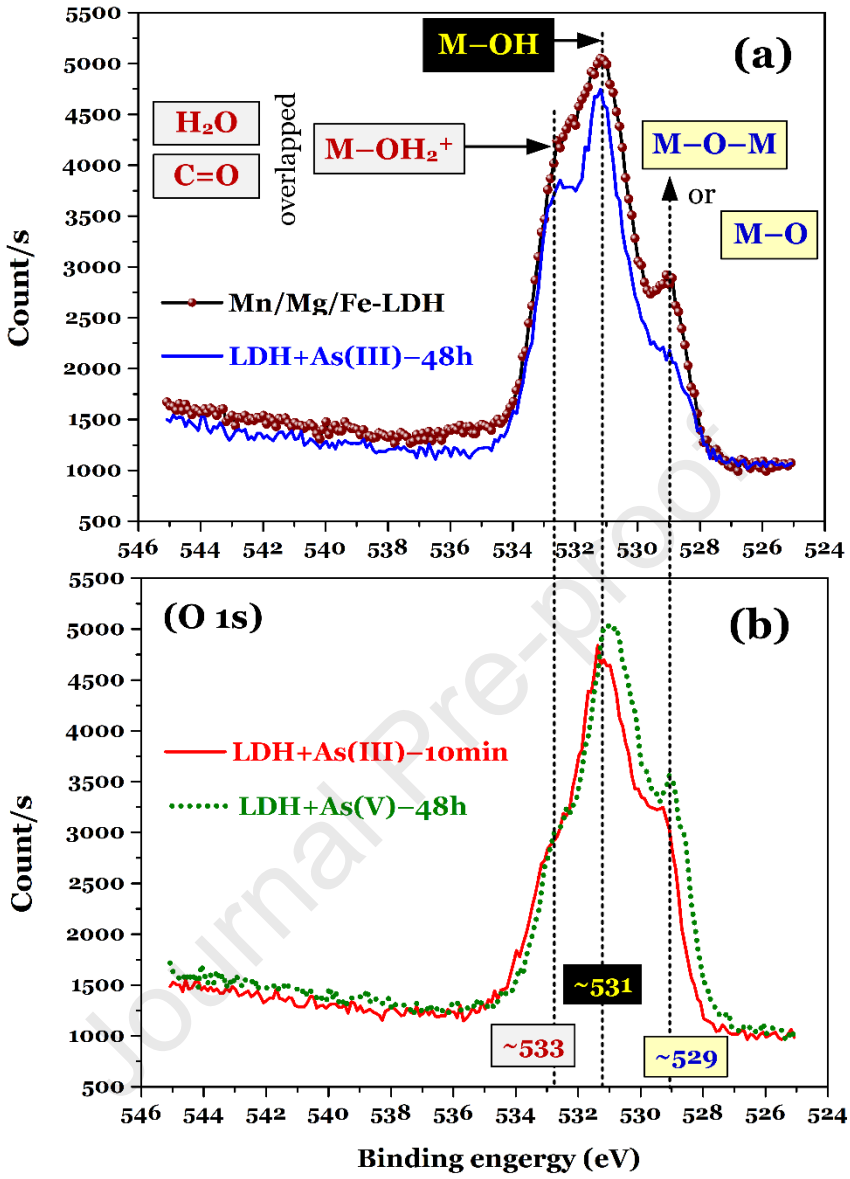

Figure 4. High-resolution spectrum of O 1s of Mn/Mg/Fe-LDH before adsorption and after adsorption **(b)** of As(III) for 10 min () As(III) for 48h, and As(V) for 48h,

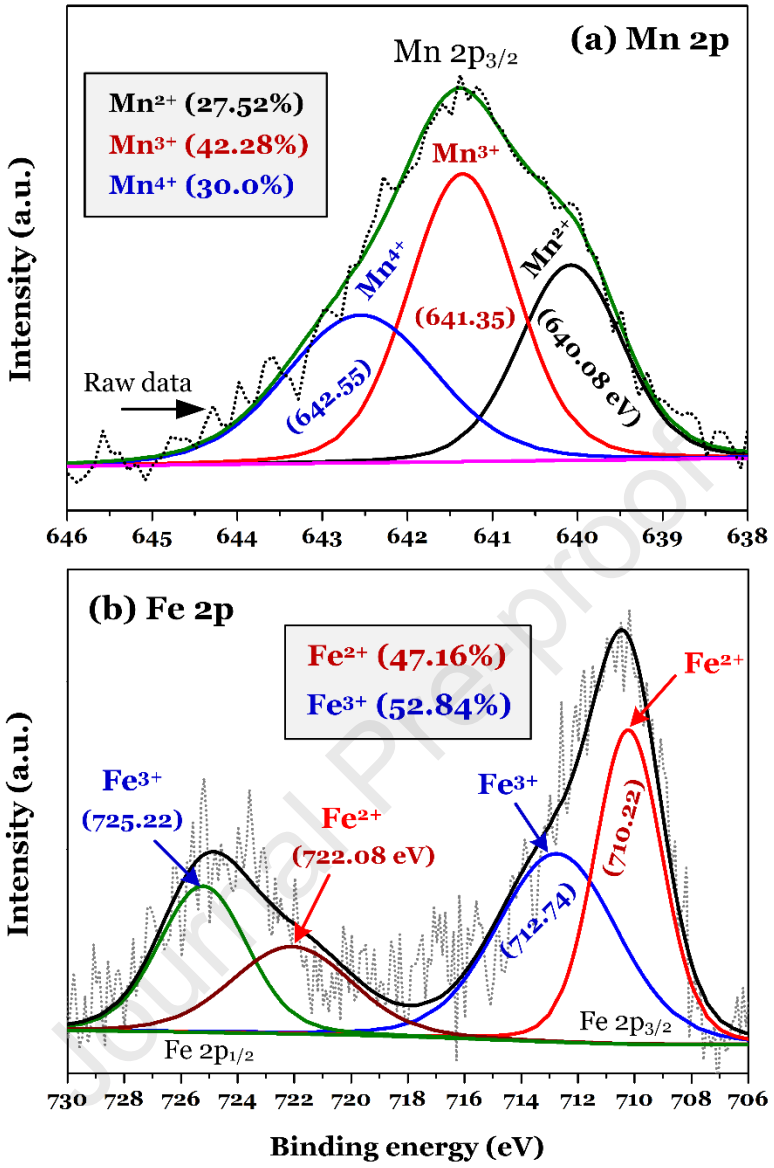

Figure 5. High-resolution spectrum of **(a)** Mn 2p and **(b)** Fe 2p of Mn/Mg/Fe-LDH

(Corresponding data for Mn/Mg/Fe-LDH after adsorption of As(III) for 10 min, As(III) for 48 h, and As(V) 48 h are presented in Figures S10 and S12)

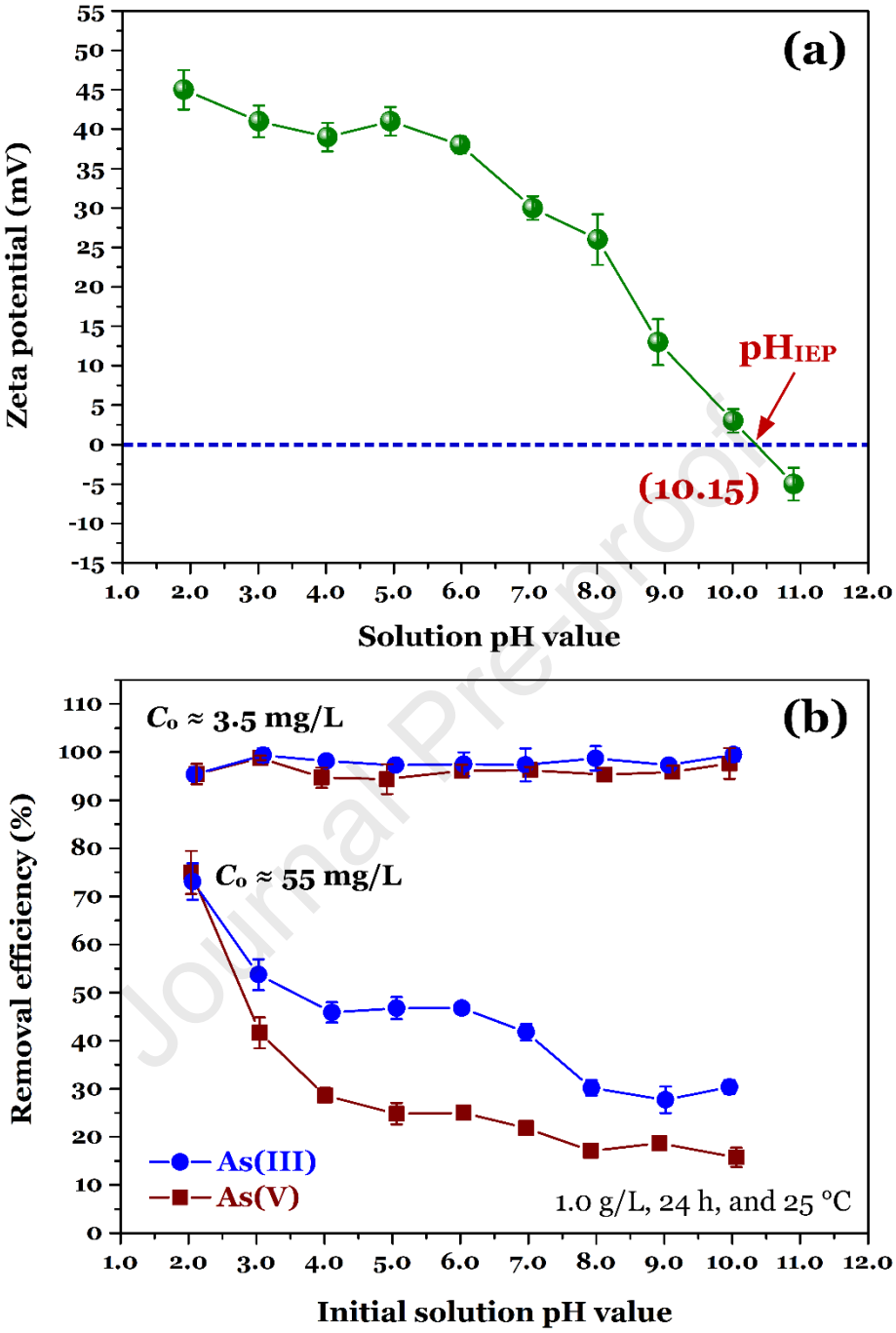

Figure 6. Effect of pH solution on **(a)** the zeta potential of Mg/Mn/Fe-LDH and **(b)** the adsorption capacity of Mg/Mn/Fe-LDH towards As(V) and As(III) ions

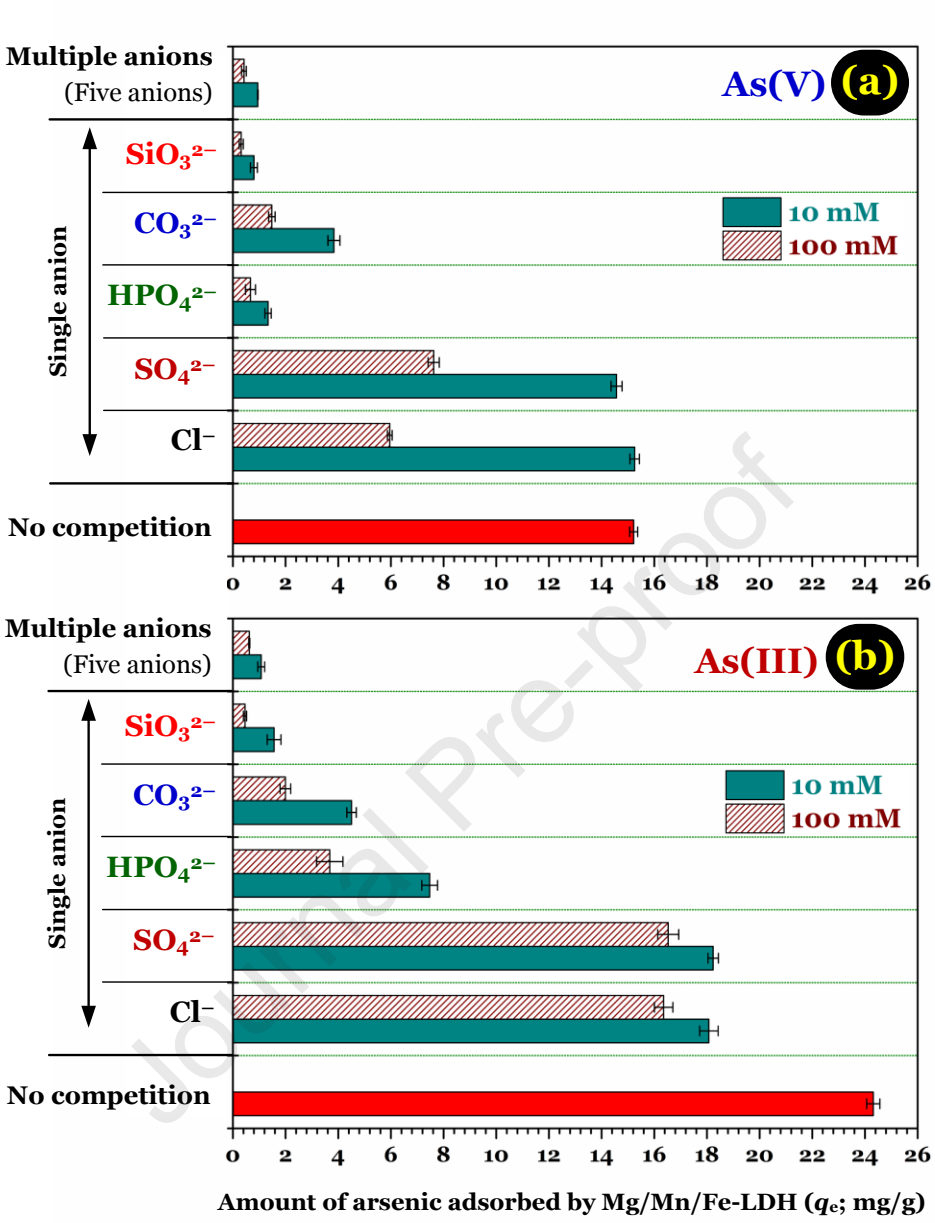

Figure 7. Effect of co-existing anions (at two concentrations of 10 mM and 100 mM) on the capacity of arsenic adsorption by Mg/Mn/Fe-LDH (Experimental conditions: $C_o \approx 50$ mg/L for As(III) or As(V), pH 7.0, 25 °C, and 24 h)

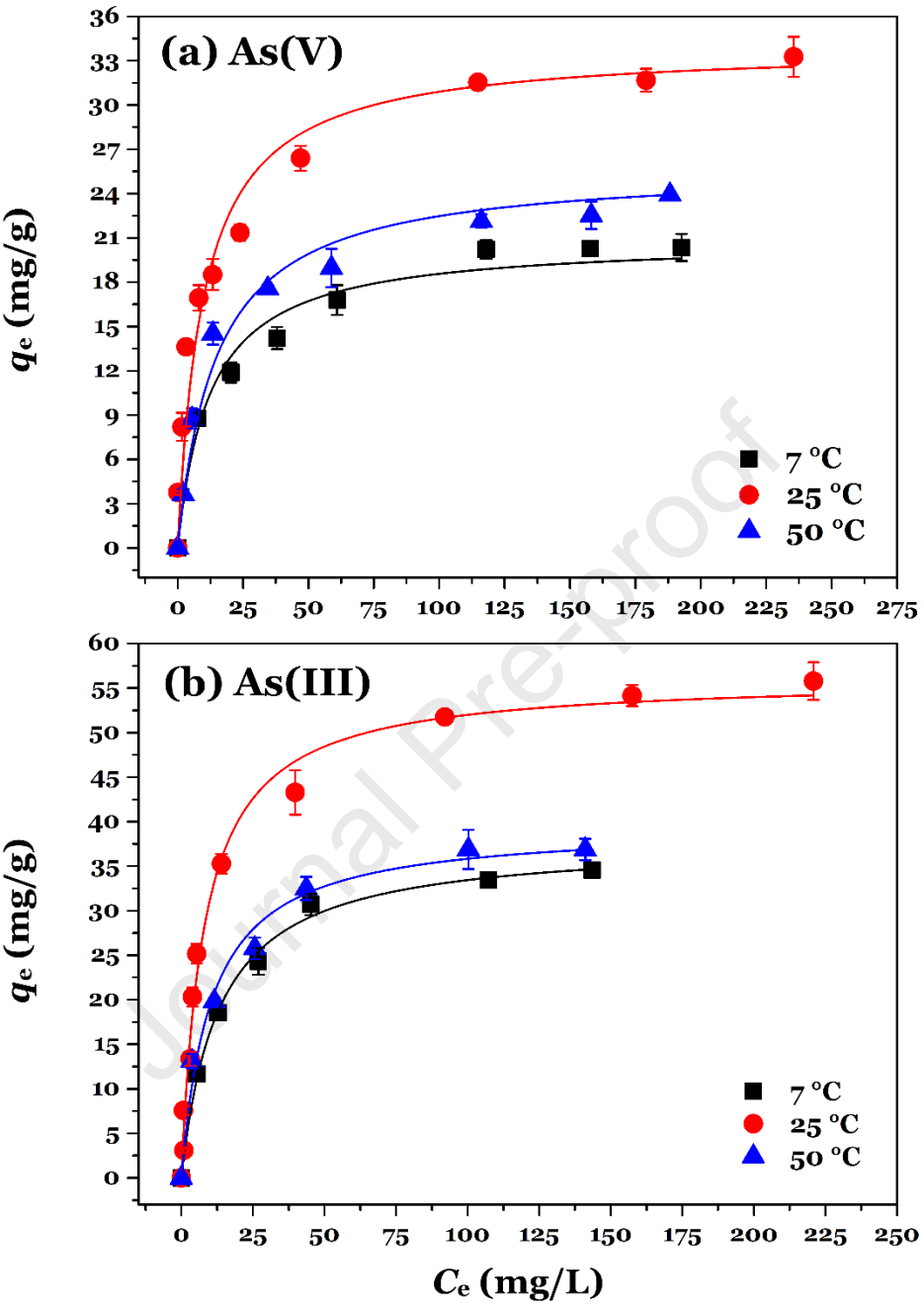

Figure 8. Adsorption isotherm of **(a)** As(V) and **(b)** As(III) onto Mg/Mn/Fe-LDH at different temperatures (Adsorption conditions: 1.0 g/L, C_o = 3.5 and 55 mg/L, 24 h, and 25 °C)

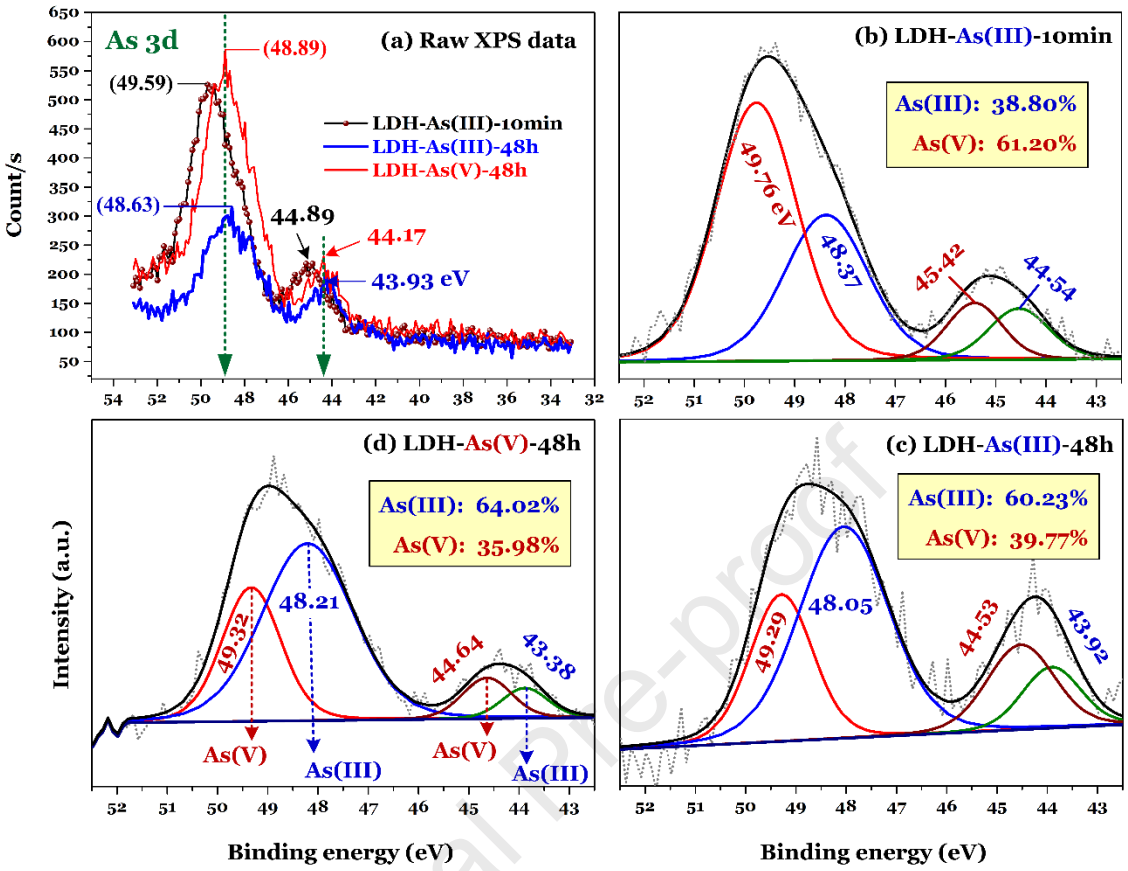

Figure 9. High-resolution spectrum of As 3d of Mn/Mg/Fe-LDH after adsorbing As(V) for 48 h [LDH-As(V)-48h], As(III) for 10 min [LDH-As(III)-10min], and As(III) for 48 h [LDH-As(III)-48h]

Highlights

- Mn/Mg/Fe-LDH: successfully synthesized through a simple co-precipitation method.
- As(III) and As(V) adsorption capacity of Mn/Mg/Fe-LDH: 56.1 mg/g and 32.2 mg/g.
- Key removal mechanism of As(III): oxidation-coupled adsorption.
- As(V) removal mechanism: inner-sphere, outer-sphere complexations, anion exchange.
- Adsorption process of arsenic ions onto Mn/Mg/Fe-LDH: highly irreversible.

Declaration of interests

☒ **The authors declare that they have no known competing financial interests or personal relationships that could have appeared to influence the work reported in this paper.**

☐The authors declare the following financial interests/personal relationships which may be considered as potential competing interests: